

VILNIUS UNIVERSITY
CENTER FOR PHYSICAL SCIENCES AND TECHNOLOGY

MARIJA MATULIONYTĖ

INVESTIGATION OF STRUCTURE AND SPECTRAL PROPERTIES
OF PHOTOLUMINESCENT GOLD NANOCCLUSERS
AND THEIR EFFECT ON CANCER CELLS

Summary of doctoral dissertation

Physical sciences, physics (02 P)

Vilnius, 2017

The study was carried out in Vilnius University during the period 2012 – 2016.

The experiments were carried out at the Biomedical Physics Laboratory of the National Cancer Institute, Lithuania (former Vilnius University Institute of Oncology).

Scientific supervisor:

Prof. habil. dr. Ričardas Rotomskis (Vilnius University, Physical Sciences, Physics – 02 P).

Doctoral dissertation will be defended at the Council of Scientific field of Physics of Vilnius University:

Chairman:

Prof. habil. dr. Valdas Šablinskas (Vilnius University, Physical Sciences, Physics – 02 P).

Members:

Prof. habil. dr. Vidas Gulbinas (Center for Physical Sciences and Technology, Physical sciences, Physics – 02 P),

Prof. dr. Edita Sužiedėlienė (Vilnius University, Physical sciences, Biochemistry – 04 P),

Prof. dr. Roaldas Gadonas (Vilnius University, Physical sciences, Physics – 02 P),

Dr. Vladimir Sivakov (Leibniz Institute of Photonic Technology, Physical Sciences, Chemistry – 03 P).

Dissertation will be defended during an open session of the Council of the Scientific field of Physics on 23rd of February, 2017 at 12:00 in the 113 Auditorium of Scientific Research Centre of National Cancer Institute, Lithuania.

Address: P. Baublio st. 3B, LT-08406, Vilnius, Lithuania.

Summary of doctoral dissertation was disseminated on 23rd of January, 2017.

Doctoral dissertation is available at the library of Vilnius University and on the VU website: www.vu.lt/lt/naujienos/ivykiu-kalendorius.

VILNIAUS UNIVERSITETAS
FIZINIŲ IR TECHNOLOGIJOS MOKSLŲ CENTRAS

MARIJA MATULIONYTĖ

FOTOLIUMINESCUOJANČIŲ AUKSO NANOKLASTERIŲ
STRUKTŪROS, SPEKTRINIŲ SAVYBIŲ BEI
POVEIKIO VĖŽINĖMS LĄSTELĖMS TYRIMAI

Daktaro disertacijos santrauka

Fiziniai mokslai, fizika (02 P)

Vilnius, 2017

Disertacija rengta 2012 – 2016 m. Vilniaus universitete.

Eksperimentiniai darbai atlikti Nacionalinio vėžio instituto (buvusio Vilniaus universiteto Onkologijos instituto) Biomedicininės fizikos laboratorijoje.

Mokslinis vadovas:

Prof. habil. dr. Ričardas Rotomskis (Vilniaus universitetas, fiziniai mokslai, fizika – 02 P).

Disertacija ginama Vilniaus universiteto Fizikos mokslo krypties taryboje:

Pirmininkas:

Prof. habil. dr. Valdas Šablinskas (Vilniaus universitetas, fiziniai mokslai, fizika – 02 P).

Nariai:

Prof. habil. dr. Vidas Gulbinas (Fizinių ir technologijos mokslų centras, fiziniai mokslai, fizika – 02 P),

Prof. dr. Edita Sužiedėlienė (Vilniaus universitetas, fiziniai mokslai, biochemija – 04 P),

Prof. dr. Roaldas Gadonas (Vilniaus universitetas, fiziniai mokslai, fizika – 02 P),

Dr. Vladimir Sivakov (Leibnico fotoninių technologijų institutas, fiziniai mokslai, chemija – 03 P).

Disertacija bus ginama viešame Fizikos mokslo krypties tarybos posėdyje 2017 m. vasario mėn. 23 d. 12:00 val. Nacionalinio vėžio instituto Mokslinių tyrimų centro 113 auditorijoje.

Adresas: P. Baublio g. 3B, LT-08406, Vilnius, Lietuva.

Disertacijos santraukos išsiųstos 2017 m. sausio mėn. 23 d.

Disertaciją galima peržiūrėti Vilniaus universiteto bibliotekoje ir VU interneto svetainėje adresu: www.vu.lt/lt/naujienos/ivykiu-kalendorius

Abbreviations

AFM – atomic force microscopy
Au NC(s) – gold nanocluster(s)
Au NP(s) – gold nanoparticle(s)
BSA – bovine serum albumin
DHLA – dihydrolipoic acid
DMEM – Dulbecco's Modified Eagle Medium
DMF – dimethylformamide
DNA – deoxyribonucleic acid
DPA – D-penicillamine
DPBS – Dulbecco's phosphate buffered saline
FA – folic acid
FL – fluorescence
HOMO – the highest occupied molecular orbital
LSPR – localized surface plasmon resonance
LUMO – the lowest unoccupied molecular orbital
MES – 2-(N-morpholino)ethanesulfonic acid
PAMAM dendrimers – polyamidoamine dendrimers
PBS – phosphate buffered saline
PEG – polyethylene glycol
PL – photoluminescence
QY – quantum yield
QD(s) – semiconductor quantum dot(s)
ROS – reactive oxygen species
SPR – surface plasmon resonance
TBHP – *tert*-butyl hydroperoxide
UV/Vis/NIR – ultraviolet/visible/near infrared light

CONTENTS

Abbreviations	5
1. INTRODUCTION.....	8
1.1. The aim of the study and objectives.....	9
1.2. Scientific novelty and actuality	10
1.3. Defended statements	12
1.4. List of publications.....	13
2. MATERIALS AND METHODS	16
2.1. Synthesis of Au NCs.....	16
2.1.1. Synthesis of BSA-Au NCs	16
2.1.2. Synthesis of Au-MES NCs	17
2.2. Spectroscopic characterization of Au NCs	18
2.3. Photostability measurements.....	18
2.4. Measurements of spatial characteristics of Au NCs	19
2.4.1. Hydrodynamic size measurements	19
2.4.2. Atomic force microscopy measurements	20
2.4.3. Transmission electron microscopy measurements	20
2.5. Cell culturing.....	21
2.6. Confocal fluorescence imaging of Au NCs in cancer cells	21
2.7. Cell viability assay	22
2.8. Cellular uptake and intracellular ROS generation of Au NCs	22
3. RESULTS AND DISCUSSION	24
3.1. Optical properties of Au NCs.....	24
3.1.1. Optical properties of BSA-Au NCs	24
3.1.2. Optical properties of Au-MES NCs.....	25
3.2. Size evaluation of Au NCs.....	26
3.2.1. Size evaluation of BSA-Au NCs	26

3.2.2. Size evaluation of Au-MES NCs.....	29
3.3. Photostability of Au NCs	30
3.3.1. Photostability of BSA-Au NCs.....	30
3.3.2. Photostability of Au-MES NCs	34
3.4. Accumulation of Au NCs in live cancer cells.....	39
3.5. Cytotoxicity of Au NCs	44
3.6. ROS generation of Au NCs in cancer cells.....	46
4. CONCLUSIONS	48
5. SANTRAUKA (Summary in Lithuanian).....	49
ACKNOWLEDGEMENT	58
6. REFERENCES	59
<i>Curriculum Vitae</i>	65

1. INTRODUCTION

Cancer is the leading cause of death in the developed countries with aging populations and worldwide. According to the statistics of WHO (World Health Organization), ~14 new cases were diagnosed in 2012. Moreover, the 70 % increase in new cases *per annum* is expected over the next 2 decades [1]. The increasing economic burden of cancer is mainly due to the inefficient diagnosis of tumours at their early stage. In order to improve the survival rates and to increase the quality of life of the diseased, it is of great importance to design novel and multifunctional probes for the accurate early diagnosis and efficient *in situ* therapy of cancer.

Nanomedicine is one of the most promising biomedical technologies of the 21st century. It uses nano-sized tools – nanoparticles with unique properties – for the diagnosis, prevention and treatment of disease. Small size, biocompatibility, unique optical and magnetic properties make nanoparticles very promising diagnostic markers, drug delivery systems as well as therapeutic agents in biomedicine [2, 3]. In the past decade noble metal nanoparticles, especially those synthesized from gold, attracted considerable interest due to tuneable optical properties, low toxicity and facile surface modification with antibodies, biomarkers and other functional molecules [4]. Therefore, gold nanoparticles have been considered very promising contrast agents in roentgenography as well as thermotherapy agents in targeted cancer therapy [2, 5].

Ultras-small photoluminescent gold and silver nanoclusters composed of several atoms with sizes up to a few nanometres is a new class of molecule-like photoluminescent probes for biomedical diagnostics and therapy [6]. They not only exhibit excellent stability but also high biocompatibility and low toxicity.

Optical properties and interaction with cells and organisms define the efficacy and applicability of nanoparticles in biomedical diagnostics and therapy.

However, despite the great improvement in the field of synthesis of Au NCs, photostability of ultra-small nanoclusters and their interaction with cells remain poorly understood.

1.1. The aim of the study and objectives

The aim:

To investigate the applicability of photoluminescent Au-MES and BSA-Au gold nanoclusters as fluorescent probes for cancer diagnostics.

Objectives:

1. To investigate structure and spectral properties of Au-MES and BSA-Au NCs.
2. To investigate stability of Au-MES and BSA-Au NCs under UV/Vis irradiation.
3. To compare accumulation of Au-MES and BSA-Au NCs in breast cancer cells.
4. To compare the effect of Au-MES and BSA-Au NCs on viability of breast cancer cells.
5. To compare the effect of Au-MES and BSA-Au NCs on generation of reactive oxygen species in breast cancer cells.

1.2. Scientific novelty and actuality

Annual growth of new cancer cases in Lithuania and worldwide motivate scientists from various fields to unite for the common goal – the search of the new more effective methods for early cancer diagnostics and treatment.

Bioimaging is one of the frontiers in biomedical sciences and has significant impact in clinical and medical research. Optical diagnostics are widely used in biomedicine for spectroscopic, flow cytometry, clinical chemistry, immunology analysis, biosensors, and image-guided surgery [7-11]. These methods are based on imaging using fluorescent markers.

Small organic molecules were the first and most widely used fluorescent markers. They exhibit high quantum yield, are easily conjugated with specific molecules and are relatively cheap [12]. Despite the fact that organic dyes are still widely used for bioimaging, their application for *in vivo* imaging is limited due to low photostability [13, 14].

Photostability is one of the key characteristics of fluorescent markers, since UV/Vis irradiation is used to excite the fluorescence of the markers. Even low-intensity continuous irradiation may result in photo bleaching and photo degradation of the fluorescent marker. The later may have crucial impact on toxicity of the markers. Searching for the fluorescent markers that would exhibit superior optical characteristics and better stability in comparison with organic fluorescent dyes, ultrasmall nanoparticles with unique properties were considered [2, 15]. Photoluminescent semiconductor quantum dots have been investigated as promising fluorescent markers for a while now. They exhibit high quantum yield and are highly more resistant to photo bleaching than organic fluorescent dyes [16]. However, QDs are usually composed of toxic chemical elements and are too large to be cleared from the organism due to many stabilizing layers [17]. Therefore, as in early 2000 the first water-soluble photoluminescent noble-metal nanoclusters were synthesized [6], they gained lots of attention. Photoluminescent silver and gold nanoclusters exhibiting molecule-like properties is a new class of fluorescent probes. Due to their facile synthesis, easy surface modification, biocompatibility and low toxicity they are very promising fluorescent markers for biomedical diagnostics and therapy as well as for biology research. [18, 19].

Even though photoluminescent Au NCs are usually considered to have stable optical properties, there are only a few publications on photostability of Au NCs [20-25]. It was reported that under irradiation with UV/Vis light some photoluminescent Au NCs retain their optical properties [20-22], yet others exhibit photobleaching [23-25]. In most of the publications only changes of photoluminescence intensity and not the shape of the spectrum were analysed, therefore the effect of UV/Vis irradiation on photoluminescent Au NCs remains poorly understood.

The cellular uptake and toxicity of large Au nanoparticles vary greatly depending on the size, shape, coating ligands and surface charge [26, 27]. Yet, despite the great improvement in the field of Au NCs synthesis, interaction of ultra-small photoluminescent gold nanoclusters with cells and other biological objects lacks deeper knowledge. Therefore, the assessment of the biocompatibility and potential toxicity of gold nanoclusters is of major importance before their clinical application.

In this study for the first time photostability, cellular uptake, cytotoxicity, and intracellular generation of reactive oxygen species of bovine serum albumin-encapsulated (BSA-Au NCs) and 2-(N-morpholino) ethanesulfonic acid (MES)-capped photoluminescent gold nanoclusters (Au-MES NCs) were investigated.

1.3. Defended statements

1. From spectral characteristics and size measurements performed and using a free electron gas model it was determined, that the size of the BSA-encapsulated photoluminescent gold nanoclusters are no bigger than 1.3 nm and that nanocluster consists of 29 gold atoms on average, meanwhile, 2-(N-morpholino)ethanesulfonic acid coated gold nanoclusters are no bigger than 0.5 nm and consist of 9 gold atoms on average.
2. Spectral properties of BSA-Au and Au-MES NCs changes under irradiation with UV/blue light, showing that photoluminescent gold nanoclusters degrade. Degradation of BSA-Au NCs is irradiation wavelength-dependent: Under irradiation with 405 nm wavelength light, gold nanocluster loses 1-2 gold atoms, while under irradiation with 280 nm, 3-4 atoms are lost.
3. Photoluminescent BSA-Au NCs and Au-MES NCs accumulate in cancer cells. Smaller photoluminescent Au-MES NCs distribute diffusely within MCF-7 and MDA-MB-231 cells including cell nuclei, while photoluminescent BSA-Au NCs accumulate in vesicles at the perinuclear region.
4. 24 hours incubation with BSA-Au NCs did not affect viability of MCF-7 and MDA-MB-231 cancer cells, yet Au-MES NCs induced incubation time dependent cytotoxicity effect on cancer cells.
5. Incubation with Au-MES NCs increased intracellular generation of reactive oxygen species in MCF-7 and MDA-MB-231 cancer cells, while incubation with BSA-Au NCs did not induce statistically significant increase in intracellular generation of reactive oxygen species in MCF-7 cancer cells.

1.4. List of publications

Publications included in Thomson Reuters Web of Science database:

1. M. Matulionyte, L. Budenaite, G. Jarockyte, D. Dapkute, R. Rotomskis. Photoluminescent gold nanoclusters in cancer cells: cellular uptake, toxicity and generation of reactive oxygen species. *International Journal of Molecular Sciences*. (Recenzuojamas)
2. V. Poderys, M. Matulionyte-Safine, D. Rupsys, R. Rotomskis. Protein stabilized Au nanoclusters: spectral properties and photostability. *Lithuanian Journal of Physics* **55**(1): 55-65 (2016).
3. M. Matulionyte, R. Marcinyte, R. Rotomskis. Photoinduced spectral changes of photoluminescent gold nanoclusters. *Journal of Biomedical Optics* **20**(5): 051018 (2015).
4. V. Pašukoniene, A. Mlynska, S. Steponkiene, V. Poderys, M. Matulionyte, V. Karabanovas, U. Statkute, R. Purviniene, J. A. Krasko, A. Jagminas, M. Kurtinaitiene, M. Strioga, R. Rotomskis. Accumulation and biological effects of cobalt ferrite nanoparticles in human pancreatic and ovarian cancer cells, *Medicina-Lithuania* **50**(4): 237-244 (2014).
5. R. Marcinyte, M. Matulionyte, R. Rotomskis. Stability and photostability of MES capped gold nanoparticles. *Proceedings of 10th International Conference and Workshop "Medical Physics in the Baltic states"* **10**: 62-66 (2012).

Presentations in international and national conferences

1. L. Budenaite, M. Matulionyte-Safine, D. Dapkute, R. Rotomskis. Cellular uptake and biological effect of MES- and BSA- coated photoluminescent gold nanoclusters *in vitro*. 59th International Conference for Students of Physics and Natural Sciences "Open Readings" 15-18 March, 2016, Vilnius, Lithuania. Abstract book p. 118.
2. L. Budenaite, M. Matulionyte-Safine, D. Dapkute, R. Rotomskis. Cellular uptake and biological effect of photoluminescent gold nanoclusters on cancer cells. International conference "Vita Scientia", 4 January, 2016, Vilnius, Lithuania. Abstract book p. 30.

3. L. Budenaite, G. Jarockyte, M. Matulionyte-Safine, R. Rotomskis. Intracellular accumulation and cytotoxicity of photoluminescent gold nanoclusters in breast cancer cells. International conference “CTCT-2015: Current Trends in Cancer Theranostics”, 1-3 June, 2015, Jena, Germany. Abstract book p. 70.
4. L. Budenaite, M. Matulionyte-Safine, R. Rotomskis. Cellular uptake and cytotoxicity of photoluminescent Au-MES NCs in MCF-7 cancer cells. 58th International Conference for Students of Physics and Natural Sciences “Open Readings”, 24-27 March, 2015, Vilnius, Lithuania. Abstract book p. 257.
5. M. Matulionyte-Safine, G. Jarockyte, L. Budenaite, R. Rotomskis. Cellular uptake and cytotoxicity of photoluminescent BSA- and MES- coated gold nanoclusters. 6th International Congress “Nanotechnology in Medicine and Biology BioNano-Med”, 8-10 April, 2015, Graz, Austria. Abstract book p. P6.
6. M. Matulionyte, R. Marcinonyte, R. Rotomskis. Photoinduced spectral changes of photoluminescent gold nanoclusters in aqueous media and *in vitro*. International conference “Laser Application in Life Sciences”, 29 June – 2 July, 2014, Ulm, Germany. Abstract book p. 230.
7. M. Matulionyte, R. Marcinonyte. Photoinduced spectral changes of photoluminescent gold nanoclusters and their accumulation in cancer cells. International conference “Nanotechnology: Research and Development. 15-16 May, 2014, Vilnius, Lithuania. Abstract book p. 92.
8. G. Jarockyte, D. Rupsys, M. Matulionyte, V. Poderys. Photostability of BSA-Au nanoclusters in biological media. International conference “Nanotechnology: Research and Development”, 15-16 May, 2014, Vilnius, Lithuania. Abstract book p. 86.
9. M. Matulionyte, R. Marcinonyte, R. Rotomskis. Photoinduced spectral changes of MES-capped gold nanoparticles. European society for photobiology 2013 congress, 2-6 September, 2013, Liege, Belgium. Abstract book p. 128.
10. M. Matulionyte, R. Marcinonyte, R. Rotomskis. Accumulation of photoluminescent MES-capped gold nanoparticles in MiaPaCa-2 cancer cells. International conference “Biophotonics-Riga 2013”, 26-31 August, 2013, Riga, Latvia. Abstract book p. 38.
11. M. Matulionyte, R. Marcinonyte, R. Rotomskis. Spectral properties and stability of photoluminescent gold-MES nanoparticles. 40th Lithuanian National Conference of Physics, June 10-12, 2013, Vilnius Lithuania. Abstract book p. 181.

12. R. Marcinonyte, M. Matulionyte, R. Rotomskis. Dynamics of accumulation of MES capped gold nanoparticles in cancer cells. 56th International Conference for Students of Physics and Natural Sciences “Open Readings 2013”, March 20-23, 2013, Vilnius, Lithuania. Abstract book p. 44.
13. M. Matulionyte, R. Rotomskis. Investigation of photophysical properties of gold-protein nanoclusters. International Scientific Conference „The Vital Nature Sign 2012”, Kaunas, Lithuania. Abstract book p. 15.
14. R. Marcinonyte, M. Matulionyte, R. Rotomskis. Stability and photostability of MES capped gold nanoparticles. 10th International Conference “Medical Physics in the Baltic States 2012”, Kaunas, Lithuania. Abstract book p. 62-66.

2. MATERIALS AND METHODS

2.1. Synthesis of Au NCs

2.1.1. Synthesis of BSA-Au NCs

The bovine serum albumin (BSA)-encapsulated gold nanoclusters (BSA-Au NCs) were synthesized according to previously reported procedure [28] with slight modifications [29]. Typically, aqueous HAuCl_4 solution (5 mL, 37°C , $c=5.27\times 10^{-3}$ M) was added to BSA solution (5 mL, 37°C , $c=7.53\times 10^{-4}$ M) under vigorous stirring. NaOH solution (0.5 mL, 1.0 M) was introduced 2 min later, and the reaction was allowed to proceed under vigorous stirring for 12 h at the temperature of 37°C . After 12 hours the synthesis solution exhibited bright red colour.

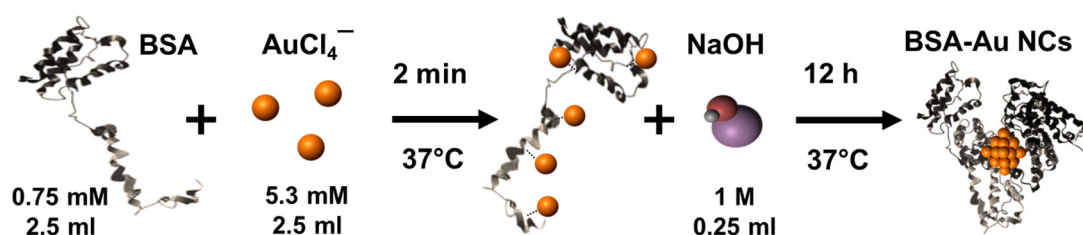


Fig. 1 Synthesis of BSA-Au nanoclusters using BSA : Au molar ratio 1:7. Adapted from [28].

It is believed that Au atoms bond to sulphur in the cysteine (Cys) residues in BSA (Fig. 1). Addition of reducing agent (NaOH) solution induces BSA folding into tertiary structure and Au atoms come close and form the nanocluster.

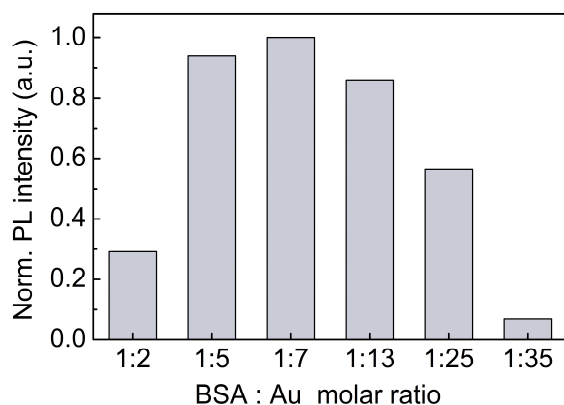


Fig. 2 Normalized photoluminescence intensity of synthesized BSA-Au NCs using different BSA : Au molar ratios.

In order to find optimal synthesis conditions we tried to use various BSA to Au molar ratios (1:2; 1:5; 1:7; 1:13; 1:25; 1:35); however, the most intense photoluminescence was observed using the BSA: Au molar ratio 1:7 (Fig. 2). All further experiments were performed using this BSA-Au NCs solution.

2.1.2. Synthesis of Au-MES NCs

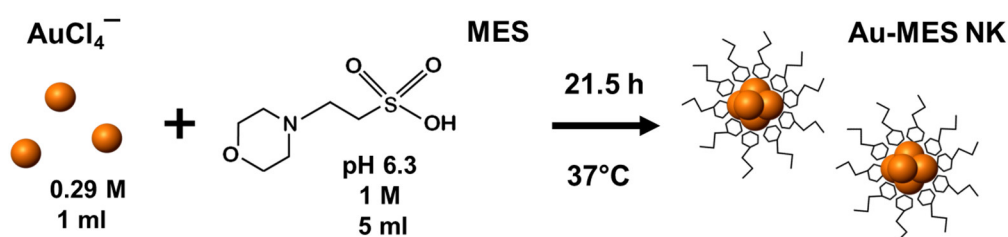


Fig. 3 Synthesis of Au-MES NCs

The gold nanoclusters capped with 2-(N-morpholino)ethanesulfonic acid (MES) (Au-MES NCs) were synthesized according to the modified synthesis protocol of Bao et al. (Fig. 3) [30]: 5 ml of aqueous MES buffer solution (1 M, pH 6.3, the pH value was achieved using NaOH) was mixed with 1 ml of chloroauric acid solution (0.29 M). Synthesis was performed under vigorous stirring for 21.5 h at the temperature of 37°C. After the synthesis solution, the Au-MES NCs were centrifuged for 30 min (10,000 rpm or $g = 6.7 \times 10^3$) with a “MiniSpin plus” centrifuge (WTW GmbH, Germany). The synthesized colloidal solution of MES-coated Au NCs exhibited a deep red colour in the daylight and greenish blue photoluminescence under UV light.

2.2. Spectroscopic characterization of Au NCs

The steady state absorption and photoluminescence spectra of the Au NCs were measured using UV-visible absorption spectrometer Varian Carry 50 (Varian Inc., Australia) and fluorescence spectrometer Varian Cary Eclipse (Varian Inc., Australia). Hellma Optik (Jena, Germany) quartz cuvettes (an optical path length 1 cm) were used for all optical measurements.

Photoluminescence of BSA-Au NCs was measured using 405 nm excitation wavelength and 10 nm excitation and emission slits. PL excitation spectra were measured at 660 nm using 430-1100 nm emission filter.

Photoluminescence of Au-MES NCs was measured using 405 and 420 nm excitation wavelengths, PL excitation spectrum was measured at 476 nm.

Photoluminescence and PL excitation spectra presented in the Results section were normalized according to the Absorption values at the excitation wavelength.

2.3. Photostability measurements

Photostability measurements of Au NCs were performed by irradiating 2 ml of the sample solution in a 1 cm path length quartz cuvette with an optical fibre coupled xenon (Xe) lamp MAX-302 (Asahi spectra Inc., Japan) or a continuous wave diode laser ($\lambda = 405$ nm, $I = 50$ mW/cm²). When irradiating with Xe lamp 280/32 nm, 330/8 nm, 366/11 nm, 402/10 nm, 470/7 nm and 492/14 nm bandpass filters were used (Fig. 3).

Photostability of Au-MES NCs was investigated irradiating the sample solution with Xe lamp using 402, 330, 366, and 470 nm bandpass filters. The collimated beam irradiated 1 cm² of the cuvette surface area with a 20 mW light power. The irradiation dose was calculated as the light intensity multiplied by the irradiation time. For all the wavelengths, a total irradiation dose of ~ 100 J/cm² was accumulated. The PL intensity of Au-MES NPs was normalized according to absorbance at the PL excitation wavelength ($\lambda_{\text{ex}} = 405$ nm). Absorption difference spectra were calculated by subtracting the absorption spectrum of Au-MES NPs solution measured before irradiation from the absorption spectrum of Au-MES NPs solution measured after a particular irradiation dose was accumulated.

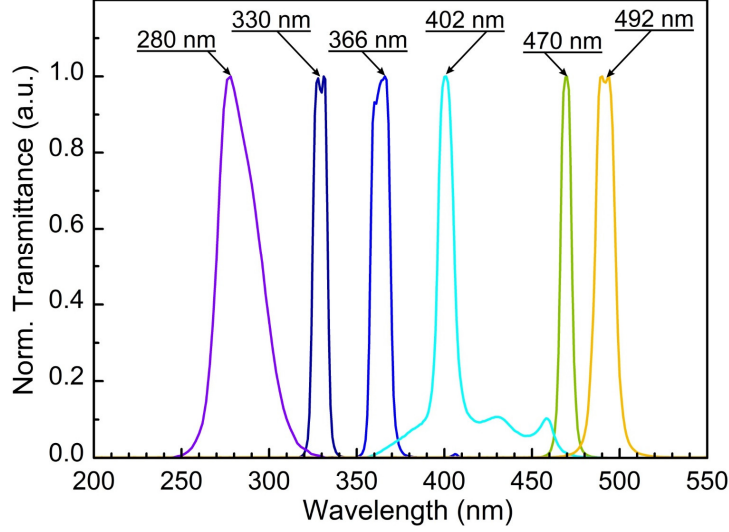


Fig. 4 Optical transmission spectra of the filters used for irradiation with Xe lamp

The photostability of BSA-Au NCs was measured by irradiating the sample solution with Xe lamp using 280 nm ($I = 7 \text{ mW/cm}^2$) and 492 nm ($I = 24 \text{ mW/cm}^2$) bandpass filters or a continuous wave diode laser ($\lambda = 405 \text{ nm}$, $I = 50 \text{ mW/cm}^2$).

The irradiation dose D (J/cm^2) was calculated as:

$$D = \frac{P \cdot t}{S} \quad (1)$$

where P – power of the light source (mW), t – irradiation time (s), and S – irradiated area of the sample (cm^2). Relative irradiation dose D_R (J/cm^2) was calculated as:

$$D_R = \frac{(1 - T) \cdot P \cdot t}{S} \quad (2)$$

where T – transmission of the sample at the irradiation wavelength, P – power of the light source (mW), t – irradiation time (s), and S – irradiated area of the sample (cm^2).

2.4. Measurements of spatial characteristics of Au NCs

2.4.1. Hydrodynamic size measurements

Hydrodynamic diameter was measured using dynamic light scattering device Zeta Plus PALS (Brookhaven Inc., USA). The method is based on photon correlation spectroscopy of quasi-elastically scattered light. Light from the laser light source ($\lambda = 660 \text{ nm}$) illuminates the sample in the cell and scattered light is registered in the detector fixed at some angle with respect to the direction of the incident light beam. Small particles in suspension undergo random thermal motion known as Brownian motion and the intensity fluctuations

of the light scattered by the particles is measured as a function of time. The decay times of the fluctuations are related to the diffusion coefficient and, therefore, the sizes of the particles. Small particles moving rapidly cause faster decaying fluctuations than large particles moving slowly. The diffusion coefficient D is inversely proportional to the particle size d :

$$D = \frac{k_B T}{3\pi \cdot \eta(t) \cdot d} \quad (3)$$

where k_B is Boltzmann's constant, T is absolute temperature in Kelvins, $\eta(t)$ is the viscosity of the solvent. This equation assumes that the particles are moving independently of one another.

The hydrodynamic radius is also known as a hydrodynamic unit. The hydrodynamic unit consists of the particle itself and the layer(s) of the ions or other small molecules adsorbed on the surface usually due to electrostatic interaction [31].

The hydrodynamic size distribution represents the average of 8 repeated measurements.

2.4.2. Atomic force microscopy measurements

Atomic force microscopy measurement were performed with VEECO diInnova atomic force microscope (VEECO Inc., USA) in tapping mode (1 Hz, 9.7 nm step) using silicon nitride probes MPP12283 (Veeco Inc., USA). The samples were prepared by casting a drop (40 μ l) on a freshly cleaved mica surface spinning at 1000 rpm (spin coating).

2.4.3. Transmission electron microscopy measurements

Transmission electron microscopy (TEM) measurements were performed on electron transmission microscope FEI TECNAI F20 (FEI) equipped with a field emission electron gun using an accelerating voltage of 200 kV and bright field images recorded on Orius SC1000B CCD camera (Gatan Inc.). Samples for TEM measurements were prepared by letting a drop (40 μ l) of colloidal Au NCs solution dry on a holey carbon film (Mesh grid 400, Agarscientific, UK).

2.5. Cell culturing

The cell lines cultivated for *in vitro* experiment were human breast cancer cell lines MCF-7 and MDA-MB-231. MCF-7 cell line was purchased from The European Collection of Cell Cultures and MDA-MB-231 cell line – from American Type Culture Collection. Cells were cultured in cell growth medium (DMEM, Gibco, US) supplemented with 10% (v/v) fetal bovine serum (FBS) (Gibco, US), 100 U/mL penicillin, 100 mg/mL streptomycin, and 4 mM L-alanyl-glutamine (Biochrom, Germany). Cells were maintained at 37 °C in a humidified atmosphere containing 5% of CO₂. For the *in vitro* experiments, synthesized Au NCs solutions were filtered using a 0.02 mm syringe filter.

For intracellular imaging studies, cells were seeded into 8-chambered cover glass plate (Nunc Lab-Tek, Thermo Fisher Scientific, US) with a density of 4×10^4 cells/chamber and subsequently incubated at 37 °C in a humidified atmosphere containing 5 % of CO₂ for 24 hours. The cells were treated with 56 mg/mL of BSA-Au NCs and 45 mg/mL of Au-MES NCs respectively then incubated under the same culture conditions for 24 hours. To investigate accumulation of pure BSA, cells were incubated with 0.01 mg/mL of BSA-Alexa Fluor 488 conjugate (Invitrogen, US) accordingly. After 24 hours of incubation the cells were washed three times with Dulbecco's phosphate buffered saline (DPBS, pH 7.0) (Sigma-Aldrich, US) and then incubated with 10 mg/mL of Hoechst 33258 (Sigma-Aldrich, Germany) solution for 30 min for staining the nuclei of the cells. After 30 min the cells were washed with DPBS and supplemented with fresh DPBS before the subsequent examination with laser scanning confocal microscope. Non-viable cells were stained with propidium iodide (incubation with 1.5 μM PI solution for 10-15 min).

2.6. Confocal fluorescence imaging of Au NCs in cancer cells

The cellular uptake of Au NCs in cells was assessed using the Nikon Eclipse Te2000-U microscope (Nikon, Japan) with the confocal laser scanning system C1si (capable of 32 bit spectral imaging). Imaging was performed using a 60×/1.4 NA oil immersion objective (Plan Apo VC, Nikon, Japan). The BSA-Au NCs, BSA-Alexa and propidium iodide were excited at 488 nm with argon-ion laser and Au-MES NCs and nucleus stain Hoechst 33258 were excited at 404 nm with diode laser. The three-channel RGB detector

(band-pass filters 450/17, 545/45 and 688/67 for blue, green and red channels, respectively) was used. The cells were maintained at 37 °C in Microscope Stage Incubation System (Okolab, Italy) in a humidified atmosphere containing 5% of CO₂ (0.80 NI/min O₂ and 0.04 NI/min CO₂). Image processing was performed using the Nikon EZ-C1 Bronze version 3.80 and ImageJ 1.46 software.

2.7. Cell viability assay

Cell viability was evaluated with the ADAM-MC automated cell counter (Digital Bio, NanoEnTek Inc., S. Korea). The cells were seeded on a 12-well plate at a density of 1×10^5 cells/well and incubated for 24 h before the nanoparticles were applied. The old medium was replaced with fresh medium containing BSA-Au NCs (56 mg/mL), Au-MES NCs (45 mg/mL), MES (0.25 M) and BSA solution (0.18 mM). The BSA concentration was the same as when incubating the cells with BSA-Au NCs. Cells incubated with medium alone were taken as control. After 24 h of incubation with BSA-Au NCs and 3, 6 and 24 h with Au-MES NCs the medium with Au NCs was carefully aspirated and the cells were trypsinized and collected in the aspirated medium and then centrifuged at $200 \times g$ for 7 minutes and resuspended in 100 μ L of phosphate buffered saline (PBS) (Gibco, UK) solution. 20 μ l of cells suspension was mixed with 20 μ l Accustain solution T and 20 μ l Accustain solution N (Digital Bio, S. Korea) for calculations of total and non-viable cells respectively. The viability was automatically calculated by the ADAM-MC software after each measurement of the total cells and the non-viable cells. The mean values of at least 3 experiments are presented.

2.8. Cellular uptake and intracellular ROS generation of Au NCs

The quantitative analysis of the cellular uptake of Au NCs and induced intercellular generation of reactive oxygen species (ROS) was assessed using flow cytometry assay.

For the evaluation of cellular uptake of BSA-Au NCs and BSA-Alexa Fluor 488 conjugate cells were seeded into 24-well culture plates (BD Falcon, USA) (5×10^4 cells per well) and subsequently incubated at 37 °C in a humidified atmosphere containing 5 % of CO₂ for 24 hours. The cells were then treated with BSA-Au NCs (56 mg/mL) and BSA-Alexa Fluor 488 conjugate (Invitrogen, US) (0,01 mg/mL) for 3, 6 or 24 h. The cells were washed

with PBS, trypsinized, and pelleted by centrifugation at $200 \times g$ for 7 minutes and resuspended in a final 100 μL volume of PBS solution for immediate analysis by flow cytometry.

For ROS generation analysis, after the treatment with Au NCs, MES and BSA solutions (concentrations used were the same as for cytotoxicity determination) the cells were washed with PBS and incubated with 5 μM CellROX Green fluorescent ROS dye (Life technologies, US) for 1 hour and then washed with PBS, trypsinized and prepared accordingly for the flow cytometry analysis. Upon oxidation, CellROX Green reagent binds to DNA and thus its signal is localized primarily in the nucleus and mitochondria. Cells treated with ROS inducer *tetr*-Butyl hydroperoxide (TBHP) (Aldrich, Germany) for 1 h under standard culture conditions were used as a positive control (400 μM). Cells treated only with fluorescent ROS dye represent negative control.

Flow cytometry was performed on Accuri C6 (Becton Dickinson, USA) flow cytometer. A minimum of 10 000 viable cells per sample were collected and analysed. CellROX Green and BSA-Alexa were visualized using argon laser (488 nm) for excitation and 530/30 band pass filter for detection. Accumulation of BSA-Au NCs was evaluated using argon laser (488 nm) for excitation, and 670 nm long pass filter for detection. The data was analysed with Flow Jo (Tree Star, USA) or Accuri C6 software.

3. RESULTS AND DISCUSSION

3.1. Optical properties of Au NCs

3.1.1. Optical properties of BSA-Au NCs

Synthesized colloidal solution of BSA-Au NCs exhibited bright red colour in the daylight and red photoluminescence under UV light. Absorption, photoluminescence (PL) and photoluminescence excitation spectra of freshly synthesized BSA-Au nanoclusters are presented in Fig. 5. Absorption of Au-BSA NCs increases in short wavelength region and has absorption band with a maximum around 278 nm, the same region where pure BSA has an absorption peak (Fig. 5). Photoluminescence spectrum of BSA-Au NCs solution has two bands in visible region. Peak positions of these bands are at 468 nm and 660 nm. PL band at 640-700 nm corresponds to photoluminescence of Au NCs that are formed inside BSA since components used for BSA-Au NCs synthesis (HAuCl_4 , BSA) or the mixture of those two materials does not have any photoluminescence band in red spectral region (600-700 nm) (data not shown). HAuCl_4 does not fluoresce at all. BSA has photoluminescence

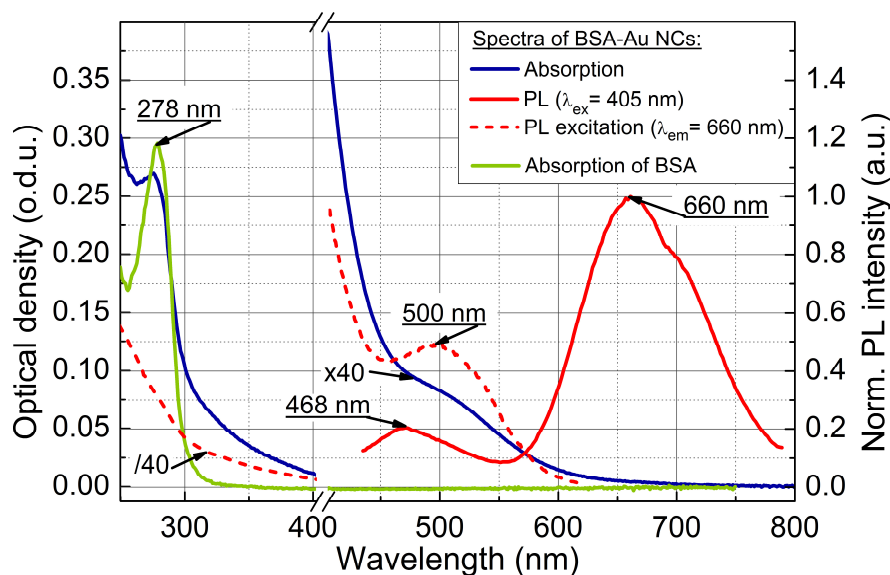


Fig. 5 Normalized absorption, photoluminescence and PL excitation spectra of BSA-Au NCs; absorption spectrum of BSA.

band around 338 nm ($\lambda_{\text{ex}} = 280$ nm), however, pure BSA also exhibits weak fluorescence in blue region at 468 nm ($\lambda_{\text{ex}} = 405$ nm) (data not shown). Photoluminescence excitation spectrum of BSA-Au NCs solution ($\lambda_{\text{em}} = 660$ nm) has a band at 500 nm and a gradual

slope to the longer wavelength region. Photoluminescence excitation spectrum does not coincide with absorption spectrum of BSA-Au NCs. Only a slight shoulder of the absorption spectrum around 500 nm was detected.

Optical properties of BSA-Au NCs solution (absorption, photoluminescence intensity, photoluminescence band position and width) remained stable for more than one month (solution was kept in dark at 4°C).

3.1.2. Optical properties of Au-MES NCs

Synthesized colloidal solution of Au-MES NCs exhibited deep red colour in daylight and blue photoluminescence under UV light. Spectral characteristics of Au-MES NCs are presented in Fig. 6.

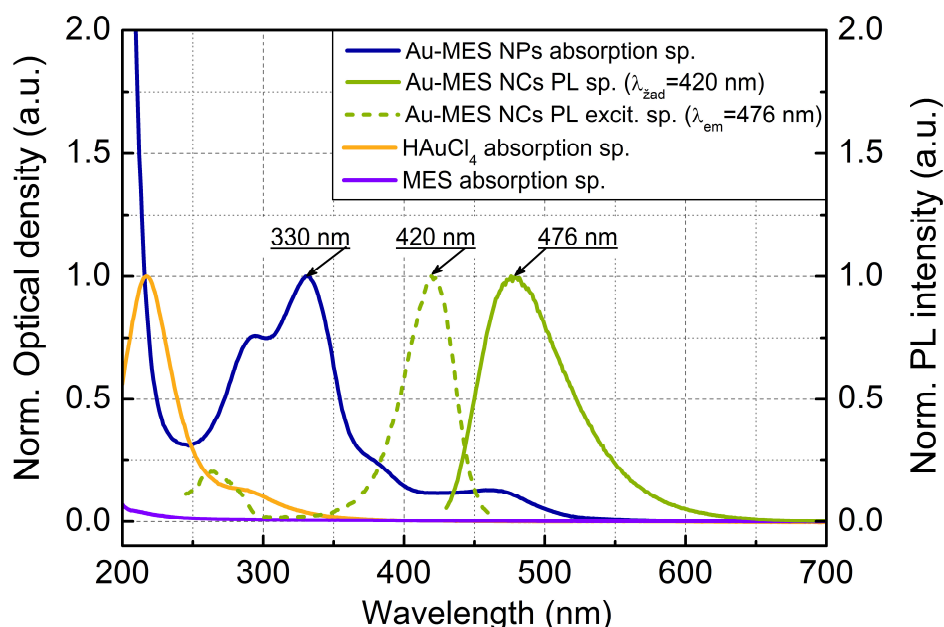


Fig. 6 Normalized absorption, photoluminescence and PL excitation spectra of Au-MES NCs; absorption spectra of HAuCl₄ and MES.

Absorption spectrum of synthesized Au-MES NPs had a main peak with a maximum at 330 nm, two peaks of lower absorbance at 290 and 475 nm, and one less expressed band at around 390 nm. Components used for the synthesis did not have absorption bands in these spectral regions. Photoluminescence of Au-MES NCs with a maximum at 476 nm wavelength ($\lambda_{\text{ex}} = 420$ nm) was detected. The photoluminescence excitation spectrum registered at the photoluminescence maximum ($\lambda_{\text{em}} = 476$ nm) had a main maximum at 420 nm and another band of lower intensity at around the 260 nm wavelength. The PL

excitation spectrum did not coincide with the absorption spectrum of Au-MES NPs. Absorption bands at 290, 330, 366 and 470 nm corresponds to absorption of non-luminescent Au-MES NPs. Nevertheless, there is no absorption in the spectral region above 510 nm that would indicate existence of gold nanoparticles exhibiting localized surface plasmon resonance (LSPR) [32-34].

3.2. Size evaluation of Au NCs

3.2.1. Size evaluation of BSA-Au NCs

The size of the nanoparticles is essential for the pharmacokinetics, biodistribution and renal clearance *in vivo* [24]. Hydrodynamic size distribution data showed that BSA-Au NCs are quite homogeneous, with diameter around 9.4 nm. In comparison, the measured hydrodynamic size of pure BSA that was approximately 6.9 nm (Fig. 7). The formation of Au NC inside the BSA results in size increase by approximately 2.5 nm.

Following a free electron gas (Jellium) model a number of gold atoms N in small gold nanoclusters can be calculated from the PL band position with a simple relation:

$$N = \left(\frac{e\lambda_{\max}E_f}{hc} \right)^3 \quad (4)$$

where e is number equal to electron charge, λ_{\max} is wavelength at emission band maximum, E_F is the Fermi energy of bulk gold (5.53 eV), h is Planck's constant and c is speed of light. From the calculations, the Au NCs exhibiting PL at 660 nm consists of 29 gold atoms on average. In literature it is reported that gold nanocluster composed of 25 atoms is less than 1 nm in diameter [35, 36]. Formation of such nanoparticle in a protein template or attached to the protein should not cause increase in BSA size by 2.5 nm. This indicates that the size increase after the synthesis could be due to the transformation of the tertiary structure of the BSA induced by formation of gold nanocluster inside the protein [37].

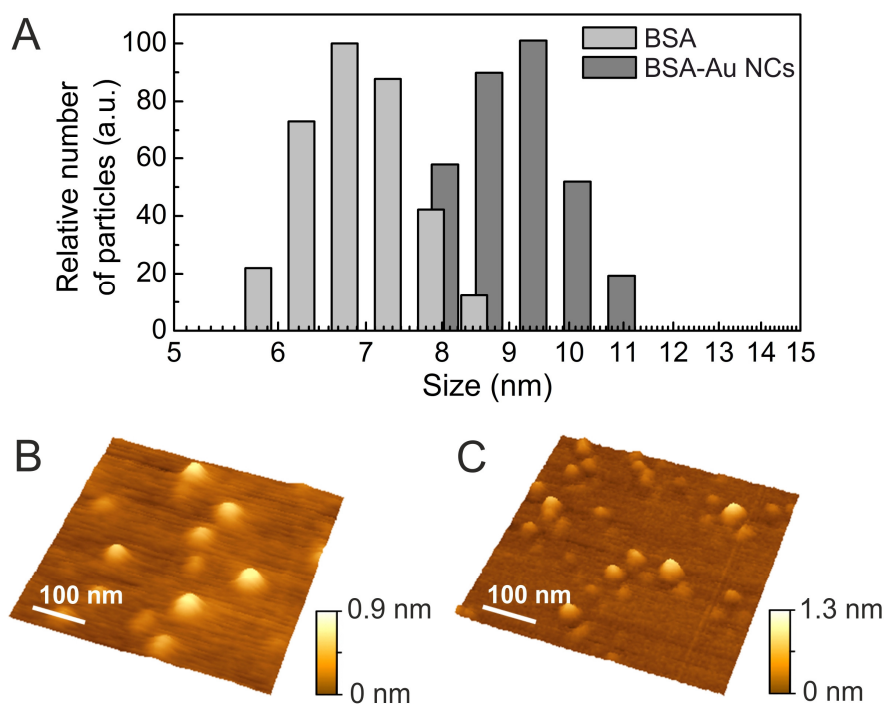


Fig. 7 Hydrodynamic size distribution of BSA-Au NCs and BSA measured using dynamic light scattering technique (A) and topography of BSA (B) and BSA-Au NCs (C) spread on mica surface measured using atomic force microscope.

AFM measurements show that BSA dispersed on mica surface loses its prolate ellipsoid structure with dimensions of $14 \times 4 \times 4$ nm [38] and flattens (Fig. 7 B). Disc shape objects of 0.9 nm in height and 30 nm in width were observed as BSA was spread on mica surface. Similar results were obtained in case of BSA-Au NCs, however, height of BSA-Au NCs was slightly bigger – approximately 1.3 nm (Fig. 7 C).

The interactions and bonds of the side chains of the amino acids that form the backbone of the protein determine its tertiary structure. Change of the surrounding medium and electrostatic interaction with hydrophilic mica surface can cause changes in BSA structure [39, 40]. Other authors have showed that adsorption of BSA on mica depends on the pH of the solution – alkaline solution results in BSA adsorption on the surface in multilayer [41]. In case of acidic pH, BSA covers mica surface in monolayer [42].

Measuring the hydrodynamic size of the particles using the dynamic light scattering method, the shape of the particles are approximated as spheres. In that case BSA-Au NCs could be approximated as the 9.4 nm diameter spheres (Fig. 8). Volume of an ellipsoid can be calculated using equation:

$$V = \frac{4}{3} \cdot \pi \cdot a \cdot b \cdot c \quad (5)$$

where a, b and c are the radiuses of an ellipsoid (in case of a sphere $a = b = c$).

If we assume that during flattening process the volume of BSA-Au NC does not change then compression of a sphere ($a = b = c = 4.7$ nm) to an oblate ellipsoid of 1.3 nm in height ($a = b, c = 0.65$ nm) leads to formation of similar structure as observed with AFM (Fig. 7). Diameter of oblate ellipsoid produced by compressing a sphere (9.4 nm in diameter) is ~ 26 nm.

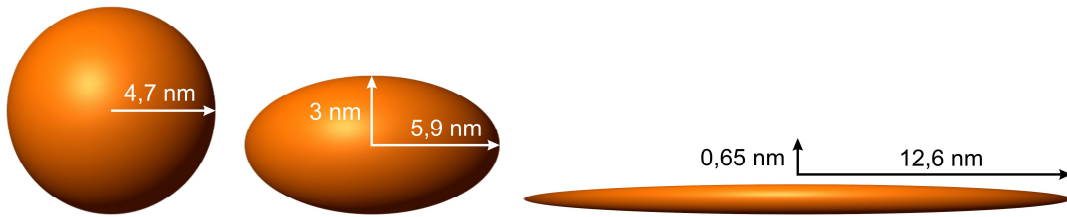


Fig. 8 Mathematical model, showing how a sphere of a size of BSA-Au NC would deform to the ellipsoid, which height equals height of the BSA-Au NCs spread on mica surface measured with atomic force microscope.

Results calculated using this model is in a good agreement with our experimental data. BSA-Au NCs dispersed on a mica surface are slightly bigger in diameter by approximately 4 nm. This can be caused by AFM “tip imaging effect“. Due to the “tip imaging” measured width of the objects is always slightly increased, therefore the differences in the diameter of pure BSA and BSA-Au NCs was not so noticeable.

The height of BSA-Au NCs spread on mica surface is only 1.3 nm, therefore it possible to conclude, that the size of gold cluster embedded into the BSA should not be bigger than 1.3 nm in diameter, because it is difficult to assume that the gold cluster can be squeezed or deformed on the mica surface.

The BSA-Au NCs retain their photoluminescence properties even when dried on glass surface which shows that the Au NCs formed inside BSA are very stable even when the conformation of the protein changes drastically.

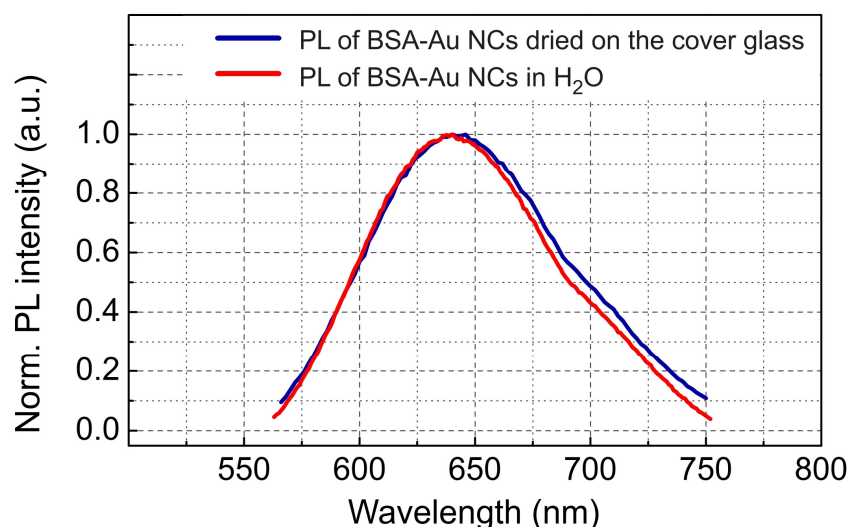


Fig. 9 PL spectrum of BSA-Au NCs dried on the glass surface in comparison with PL spectrum of BSA-Au NCs in deionized water ($\lambda_{\text{ex}} = 405 \text{ nm}$)

3.2.2. Size evaluation of Au-MES NCs

The size of Au-MES NCs was measured using atomic force microscopy and scanning transmission electron microscopy. The size of Au-MES NPs measured with atomic force microscope was 0.5-10 nm in height (Fig. 10 A). Meanwhile, the size of the nanoparticles spread on holey carbon film measured with TEM was 2-6 nm in diameter (Fig. 10 B).

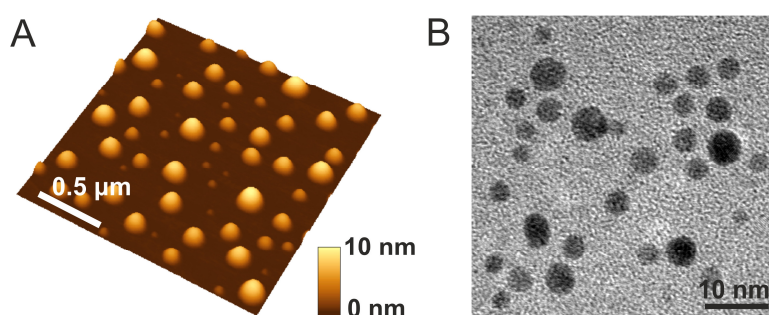


Fig. 10 Topography of Au-MES NPs on a mica surface (AFM image) (A) and STEM image of Au-MES NPs on a carbon film (B).

As it was mentioned earlier, following a free electron gas model a number of gold atoms N in small gold nanoclusters can be calculated from the PL band position (eq. 4). According to the calculations, Au NCs that exhibit photoluminescence at 476 nm wavelength

consist of ~ 9 gold atoms and is smaller than 1 nm in diameter. Such ultrasmall nanoclusters (~ 0.5 nm) were observed on a mica surface with atomic force microscope. However, no such small structure were detected in case of transmission electron microscopy, possibly due to too low contrast with the carbon film.

It is reported that localized surface plasmon resonance is exhibited by Au NPs larger than 3 nm in diameter [33]. The LSPR absorption band is clearly visible as a peak in the range between 520 and 580 nm. The LSPR absorption band position shifts to longer wavelength spectral region as the size of the NPs increases. However, even though there were larger than 3 nm NPs in Au-MES NPs solution, the LSPR absorption band was not detected in the absorption spectrum. This could be due to the fact that for small particles this peak is damped due to the reduced mean free path of the electrons [33].

3.3. Photostability of Au NCs

3.3.1. Photostability of BSA-Au NCs

Photostability of BSA-Au NCs was investigated irradiating the sample solution with three different wavelengths: 280 nm, 405 nm and 492 nm. 280 nm wavelength was chosen due to BSA absorption at this wavelength. 405 nm – the wavelength, used in microscopy for PL excitation of BSA-Au NCs. 492 nm irradiation wavelength was chosen to investigate photostability of BSA-Au NCs without directly affecting PL band at 470 nm.

The investigation of BSA-Au NCs photostability showed that the photostability depends on the wavelength of light used for irradiation of BSA-Au NCs solution with 280 nm, 405 nm and 492 nm wavelength light induced different changes in photoluminescence spectra (Fig. 11 A-C). Changes in absorption spectra were negligible. Independent of the irradiation wavelength PL intensity at 660 nm decreased and the maximum is shifted to the shorter wavelength region. There are several possible causes that could explain the decrease of the BSA-Au NCs PL intensity at 660 nm. The first one is the photo degradation of nanoclusters. Irradiation of the BSA-Au NCs sample with 405 and 492 nm wavelength light caused a hypsochromic shift of the emission band from 660 to 652 nm. According to the calculations based on Eq. 2, the hypsochromic shift of the fluorescence band by 8 nm could reflect loss of one gold atom in a cluster. Irradiation with 280 nm light causes a

larger hypsochromic shift (22 nm). Such a shift could be caused by loss of 3–4 gold atoms in Au NCs.

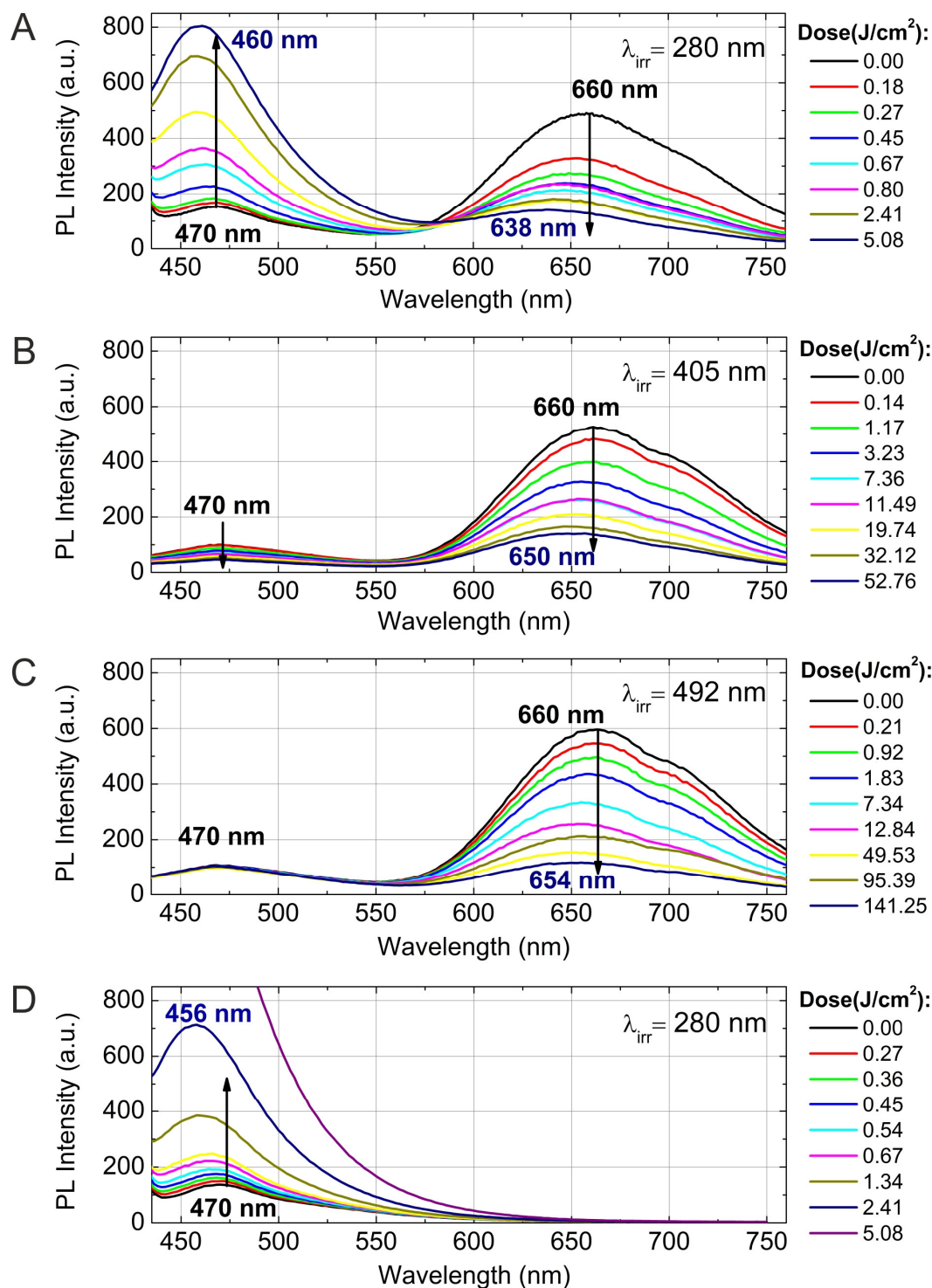


Fig. 11 Photoluminescence spectra of the BSA-Au NCs in aqueous solutions after irradiation with 280 nm (A), 405 nm (B), 492 nm (C) light and photoluminescence spectrum of BSA after irradiation with 280 nm light (D). PL emission spectra were obtained under the excitation at 405 nm. Arrows indicate spectral changes as the irradiation dose increases.

It is known that Au NCs composed of a specific number of gold atoms show high stability. These numbers are called “magic numbers”. The closest magic number to 29 is 25. Therefore, it is likely that during irradiation Au NCs degrade and more stable Au NCs composed of 25 atoms are formed, which causes a hypsochromic shift of the PL band. Another possible explanation for the PL intensity decrease and hypsochromic shift would be the deterioration of a nanoparticle coating layer. It was shown that the enzymatically generated H₂O₂ and enzymatic proteolysis induces degradation of BSA-Au NCs corona and causes a hypsochromic shift and the decrease of PL intensity [35, 43]. The degradation of a nanoparticle coating usually leads to a decrease in PL intensity [44, 45]. These two processes (nanocluster deterioration and coating degradation) can take place simultaneously and result in a hypsochromic shift of the PL band and intensity decrease under irradiation. Irradiating the samples with 492 nm all the energy is absorbed only by Au NCs as BSA has an absorption band at 280 nm, therefore, direct photo degradation of BSA is impossible. However, other authors have showed that under UV/Vis irradiation Au NCs can generate free radicals [46, 47] or singlet oxygen [48] which could lead to indirect degradation of BSA.

Irradiation of BSA-Au NCs at 280 nm leads to a much faster PL intensity decrease and a much bigger hypsochromic shift of the PL band (compared to irradiation at 492 nm). 280 nm wavelength light is strongly absorbed by both the Au NCs and the BSA coating. In this case photo degradation of Au NCs as well as of an Au NCs coating layer (BSA) can occur. Irradiation of the BSA solution with 280 nm light causes a decrease of the BSA PL band at 338 nm (data not shown). This indicates that the irradiation of BSA with 280 nm light causes photodegradation or conformational changes of BSA. Degradation of the Au NCs surface coating (BSA) makes Au NCs less protected from solvent (water) molecules and relaxation via surface defects can increase. This suggests that the degradation of BSA strongly influences the PL properties of BSA-Au NCs. The effect of irradiation on the PL band at 470 nm was completely different when compared to the PL changes of the PL band at 660 nm. Under the irradiation of BSA-Au NCs with 405 nm light PL intensity at 660 nm decreased by 73 % whilst at 470 nm it decreased by 54 %. Irradiation with 492 nm light did not cause any effect on PL band at 470 nm, yet PL at 660 nm decreased by 80 %. Under irradiation with 280 nm light the PL intensity at 470 nm increased more than 5 times, meanwhile PL intensity at 660 nm decreased by 71.5 %. Very similar

results were obtained when the pure BSA solution was irradiated with 280 nm light (Fig. 11 D): the PL intensity at 470 nm increased 10 times during irradiation. This shows that the PL band at 470 nm is not related to the Au NCs PL but it corresponds to the photo transformation of BSA. Irradiation of the pure BSA solution under identical conditions causes a bigger increase in the PL intensity at 470 nm compared to the BSA-Au NCs solution. This can be explained in two ways: i) some of irradiation light is absorbed by Au NCs and does not induce any BSA damage; ii) the excited state of BSA can be quenched by Au NCs. Both of these processes reduce the photo transformation of BSA.

BSA does not absorb 405 nm light, therefore, photo transformation of BSA was not detected when the samples were irradiated using 405 nm light. However, 405 nm light is absorbed by BSA photoproduct (PL $\lambda_{\text{max}} = 470$ nm) and could be related to their photo degradation. This leads to a decrease of the PL intensity of the PL band at 470 nm. The irradiation at 492 nm does not induce any changes in the PL band at 470 nm because BSA and BSA photoproduct do not absorb light of this wavelength.

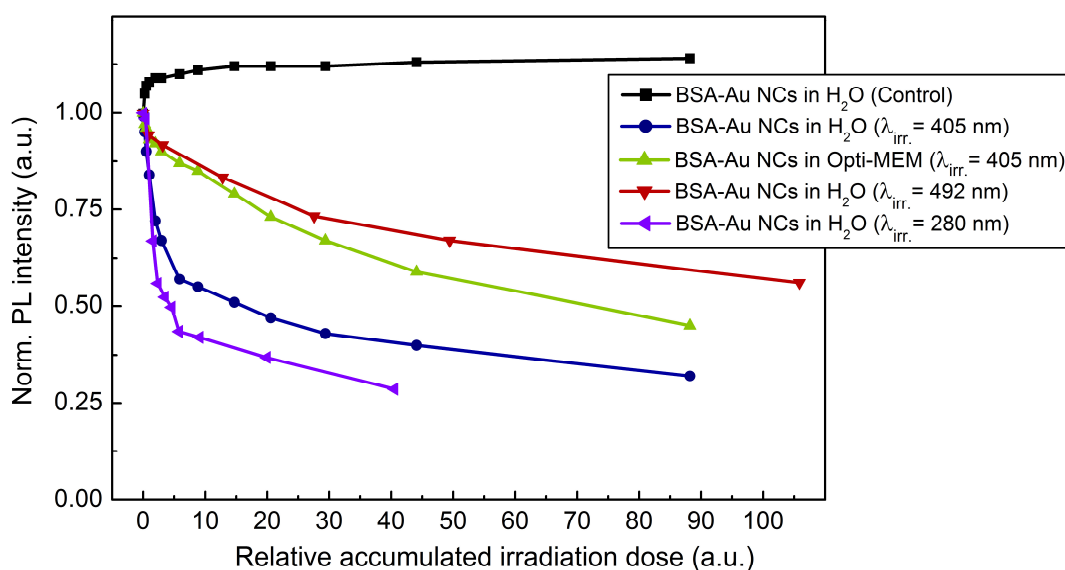


Fig. 12 Dependence of normalized PL intensity of BSA-Au NCs at 660 nm on relative accumulated irradiation dose ($\lambda_{\text{ex}} = 405$ nm). Relative accumulated irradiation dose refers to a dose divided by absorbance of BSA-Au NCs at wavelength used for irradiation.

The irradiation of BSA-Au NCs in the Opti-MEM showed that the BSA-Au NCs exhibit greater photostability in this cell culture medium (Fig. 12). The increased photostability of BSA-Au NCs in the Opti-MEM might be caused by the formation of an additional coating layer of BSA-Au NCs. The Opti-MEM medium contains proteins and amino acids.

It was shown that proteins can increase the quantum yield and stability of nanoparticles by the formation of “protein corona” around nanoparticles [44].

3.3.2. *Photostability of Au-MES NCs*

Under irradiation at around the maximum of photoluminescence excitation band of Au-MES NCs ($\lambda_{\text{irr}} = 402$ nm) slight decrease of absorbance of Au-MES NPs in 250-550 nm spectral region was detected (Fig. 13) as accumulated irradiation dose increased. Absorption difference spectra revealed several distinct bleaching absorption bands with maxima at 290, 330, 366, 420 and 470 nm. Bleaching absorption bands at 290, 330, 366 and 470 nm corresponded to the bands in the absorption spectrum of Au-MES NPs. However, no correlation in intensity of the absorption bands and the bleaching bands under irradiation with 402 nm wavelength light was observed. In addition, bleaching absorption band at 420 nm was indistinguishable in absorption spectrum and correlated with the main photoluminescence excitation band of Au-MES NCs. Simultaneously, decrease of intensity of PL band ($\lambda_{\text{ex}} = 405$ nm) with a maximum at 476 nm and hypsochromic PL band shift by 47 nm resulting in formation of a new PL band with a maximum at 430 nm was observed (Fig. 13 B). No PL band shift and only decrease in PL intensity at 476 nm was observed as 420 nm excitation wavelength was used (Fig. 13 C).

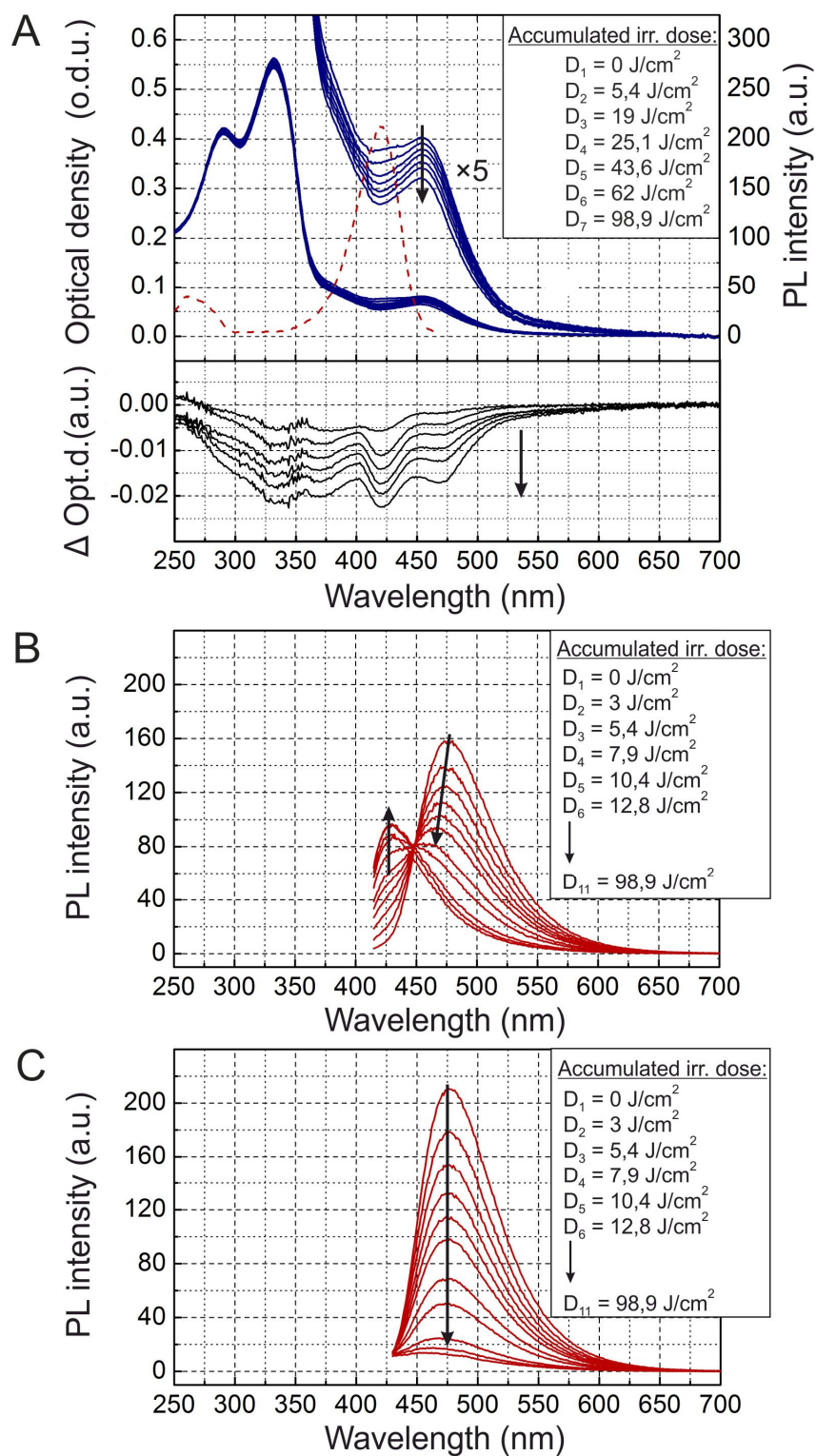


Fig. 13 Spectral changes of Au-MES NPs at $\lambda_{\text{irr}} = 402 \text{ nm}$ as accumulated irradiation dose increases. Changes of absorption spectrum (top) and absorption difference spectra (bottom) (A), PL excitation spectrum ($\lambda_{\text{em}} = 476 \text{ nm}$) (dashed curve). Changes of PL spectrum ($\lambda_{\text{ex}} = 405 \text{ nm}$) (B). Photobleaching of PL spectrum ($\lambda_{\text{ex}} = 420 \text{ nm}$) (C). Arrows represent changes in absorbance and PL intensity.

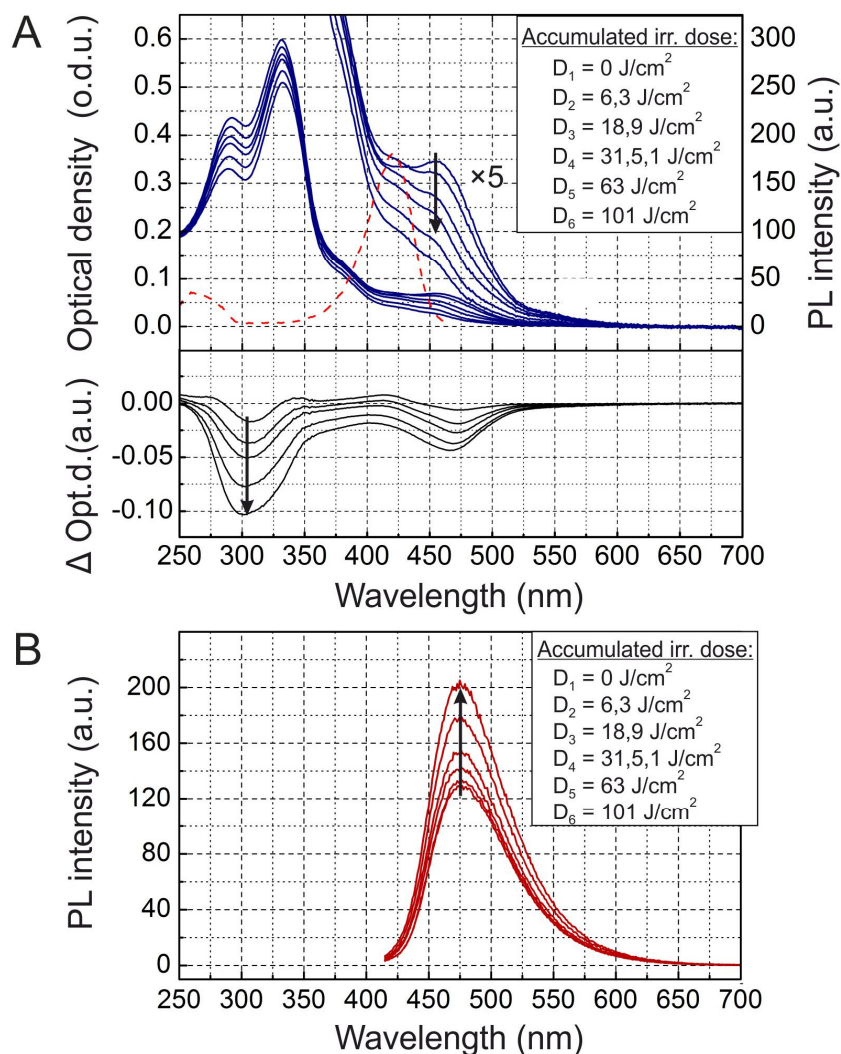


Fig. 14 Changes of absorption spectrum (top) and absorption difference spectra (bottom) of Au-MES NPs at $\lambda_{\text{irr.}} = 330$ nm as accumulated irradiation dose increases (A), PL excitation spectrum ($\lambda_{\text{em}} = 476$ nm) (dashed curve). Changes of PL spectrum ($\lambda_{\text{ex}} = 405$ nm) (B). Arrows represent changes in absorbance and PL intensity.

Irradiating Au-MES NPs solution with near-UV light at 330 nm, the most intensive decrease of absorbance was detected at around 300 nm and 470 nm (Fig. 14). At the same time increase of PL ($\lambda_{\text{ex}} = 405$ nm) intensity was observed, peak position remained intact. Under irradiation of Au-MES NPs colloidal solution with 366 nm wavelength light the most intensive decrease in absorbance was observed at around 330 and 470 nm wavelengths (Fig. 15 A). Distinct photobleaching bands were observed in absorption difference spectra at these wavelengths. PL changes (Fig. 15 B-C) were similar as in case of irradiation with 402 nm wavelength light.

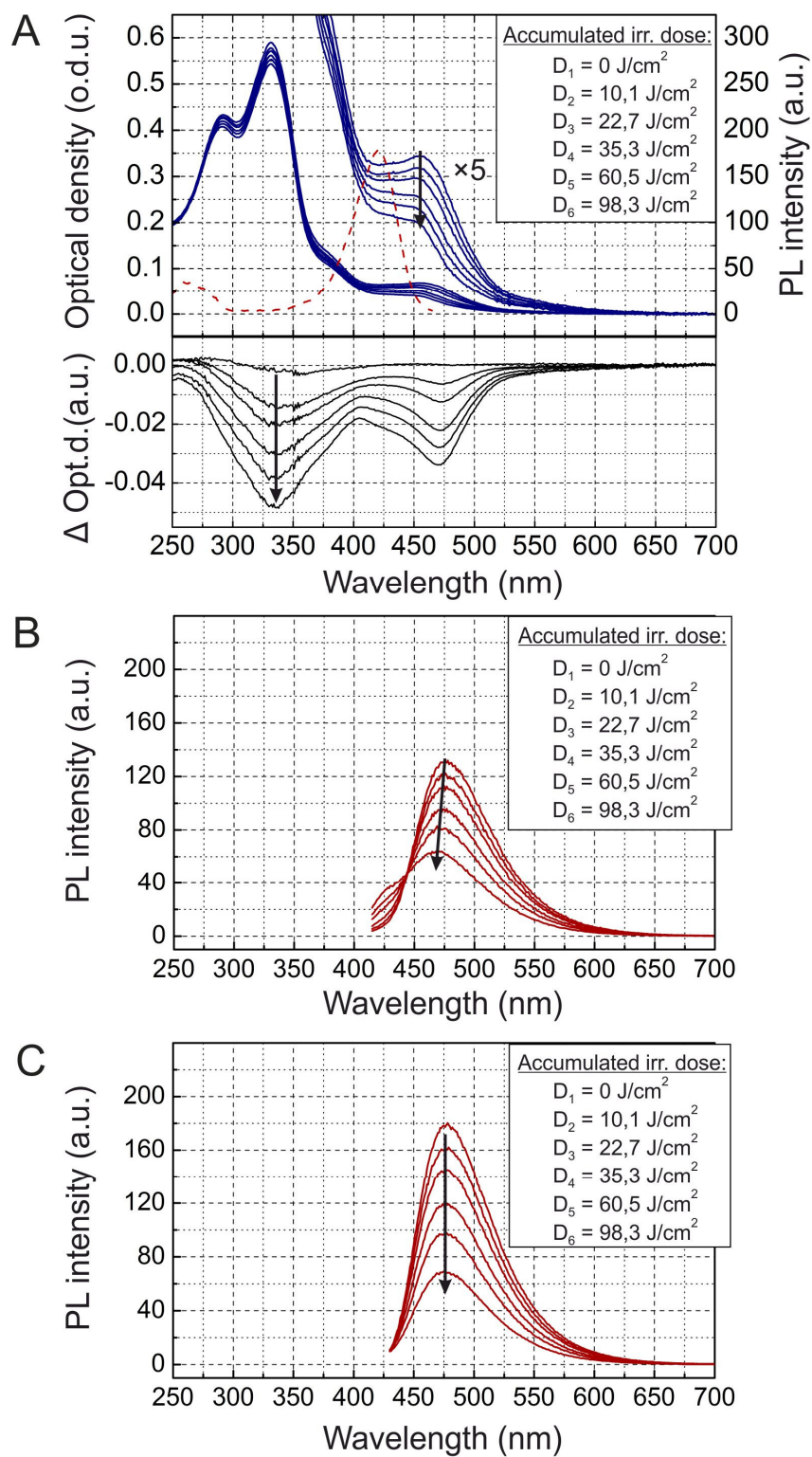


Fig. 15 Spectral changes of Au-MES NPs at $\lambda_{irr.} = 366 \text{ nm}$ as accumulated irradiation dose increases. Changes of absorption spectrum (top) and absorption difference spectra (bottom) (A), PL excitation spectrum ($\lambda_{em} = 476 \text{ nm}$) (dashed curve). Changes of PL spectrum ($\lambda_{ex} = 405 \text{ nm}$) (B). Photobleaching of PL spectrum ($\lambda_{ex} = 420 \text{ nm}$) (C). Arrows represent changes in absorbance and PL intensity.

Irradiating colloidal solution of Au-MES NPs with 470 nm wavelength light no changes in absorption and PL spectra were observed even when the maximum irradiation dose of $\sim 100 \text{ J/cm}^2$ was accumulated (data not shown).

Discrepant changes in absorption difference spectra under irradiation at different wavelengths (Fig. 16) suggests that the absorption spectrum of Au-MES NPs is a superposition of the absorption of photoluminescent Au-MES NCs and of the minimum two different fractions of non-luminescent Au-MES NPs.

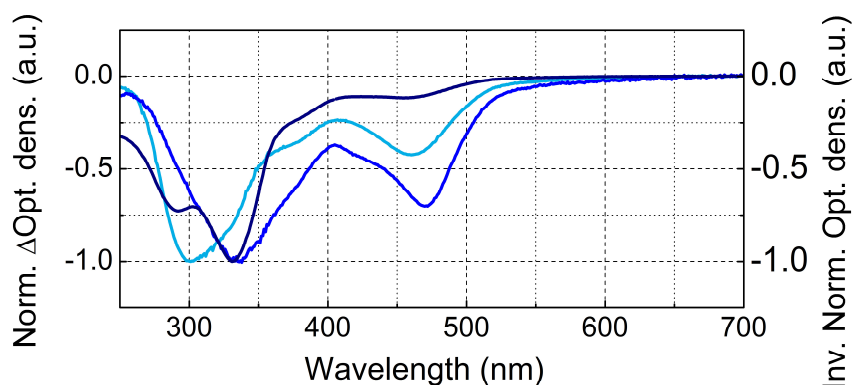


Fig. 16 Inverted normalized absorption spectrum of Au-MES NPs (dark blue) and normalized absorption difference spectra of Au-MES NPs under irradiation at 330 nm (blue) and at 366 nm (cyan).

The appearance of the bleaching band at 420 nm in the absorption difference spectrum (Fig. 13 A) that coincides with the maximum of the PL excitation spectrum and the simultaneous decrease of PL intensity at 476 nm (Fig. 13 B-C) revealed that photoluminescent Au-MES NCs were irradiation-disrupted. However, a hypsochromic shift of the PL band position and the appearance of the new PL band at 430 nm suggested that under irradiation with 402 nm wavelength light a new type of photoluminescent NCs with a PL peak at the 430 nm wavelength were formed (Fig. 13 B). Following a free electron gas model it was calculated that Au-MES NCs exhibiting PL at 476 nm consist of ~ 9 gold atoms. As the PL band maximum has shifted to 430 nm wavelength, the number of gold atoms must have decreased to 7.

Irradiating the sample solution at $\lambda_{\text{irr}}=330 \text{ nm}$ decrease of absorbance at around 300 nm occurred simultaneously with the increase in PL intensity at 476 nm (Fig. 14) indicating disruption of bigger non-luminescent Au-MES NPs and formation of photoluminescent NCs from their remains. Since PL intensity in PL excitation spectrum at 330 nm is negligible, irradiation at 330 nm did not directly affect photoluminescent Au-MES NCs.

There are no results in the literature showing that low-intensity light would reduce the size of photoluminescent gold nanoclusters, though decrease of PL intensity has been reported for dimethylformamide (DMF)-, trypsin- and dihydrolipoic acid (DHLA)- stabilized gold nanoclusters under irradiation with near-UV light [23-25]. However, irradiation of photoluminescent semiconductor QDs with UV/VIS light is well known to affect PL quantum yield [49-51] and induce continuous hypsochromic [49, 50] or bathochromic [51] shift of PL band indicating photo etching and aggregation of QDs respectively. However, discrete spectral shift of Au-MES NCs suggesting a molecule-like behaviour complicates comparison of photoluminescent Au NCs with semiconductor QDs that undergoes continuous shift of PL band under irradiation with UV/VIS light.

Low-power irradiation (20 mW) used in our experiments could not induce high energy related processes such as ablation of solid materials producing nanoclusters that can be achieved using high-energy pulsed-lasers. However, it has been shown that low-power irradiation with UV light can induce formation of gold nanoparticles from chloroauric acid. Irradiation of gold nanoparticles (17-23 nm in diameter) with low-power UV light can as well induce generation of one or a few reactive oxygen species (ROS) such as hydroxyl radicals ($\bullet\text{OH}$), singlet oxygen ($^1\text{O}_2$), superoxide radicals ($\text{O}_2^{\bullet-}$) [47, 52]. Despite the fact that Zhang and his colleagues have shown that under UV exposure of gold nanoparticles (17-23 nm in size) no gold ions were detected [52], upon irradiation with 402 nm (as with 366 nm) wavelength light size of photoluminescent gold nanoclusters (< 1 nm in diameter) decreased, irradiation at 330 nm disrupted non-luminescent NPs (< 10 nm in diameter). The greater effects on Au-MES NPs such as disruption and decrease in size could have appeared due to increased ROS generation as under irradiation with X-ray, smaller gold nanoparticles generate more ROS than bigger nanoparticles due to increased surface area to volume ratio [47].

3.4. Accumulation of Au NCs in live cancer cells

To investigate internalization of BSA-Au NCs and BSA in MCF-7 and MDA-MB-231 breast cancer cells the cells were incubated with BSA-Au NCs (56 mg/mL) and with BSA-Alexa 488 conjugate (0,01 mg/mL) respectively. After 24 hours of incubation BSA-Au NCs were observed accumulated in vesicles inside MCF-7 cancer cells (Fig. 17 a_{1,2}).

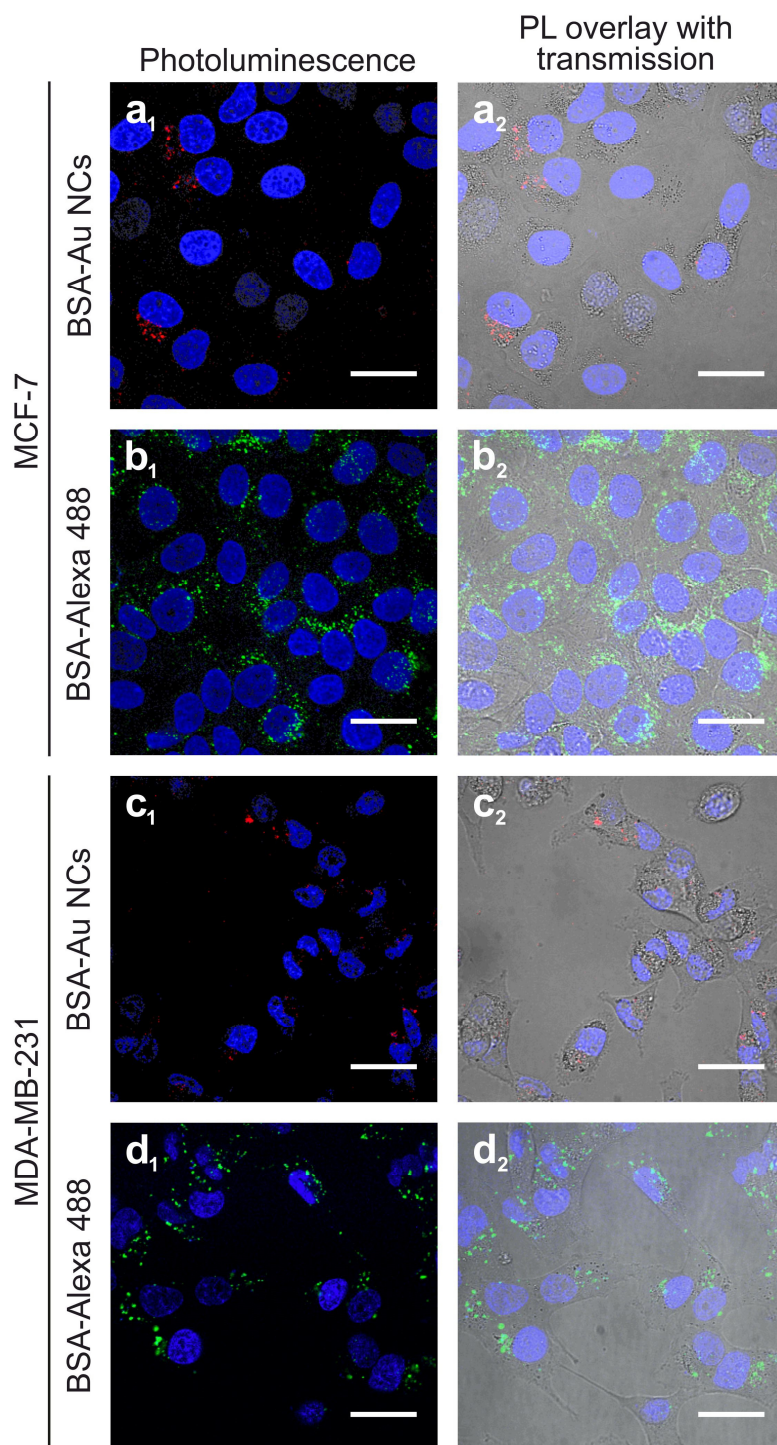


Fig. 17 Accumulation of photoluminescent BSA-Au NCs ($\lambda_{\text{ex}}=488$ nm) and BSA-Alexa conjugate ($\lambda_{\text{ex}}=488$ nm) in MCF-7 and MDA-MB-231 cells after 24 h of incubation, nuclei stained with Hoechst 33258 ($\lambda_{\text{ex}}=405$ nm). Scale bar is 30 μm

No fluorescence at this spectral region was observed in the nuclei of the cells. BSA-Au NCs did not accumulate uniformly, flow cytometry data showed that only 73.5% of the MCF-7 cells had internalized BSA-Au NCs after 24 hours of incubation (71.3% after 3 h

and 6 h of incubation respectively) (Fig. 18 A). For comparison, after 24 hours of incubation the vesicles containing fluorescent BSA-Alexa 488 conjugate were observed in all of MCF-7 cells (Fig. 17 b_{1,2}).

Flow cytometry data confirmed that 100 % of the cells had internalized fluorescent BSA-Alexa 488 conjugate after 24 hours of incubation (96.6 % and 99.5 % after 3 h and 6 h of incubation respectively) (Fig. 18 A). Accumulation of photoluminescent BSA-Au NCs ($\lambda_{\text{ex}}=488$ nm) and BSA-Alexa conjugate ($\lambda_{\text{ex}} = 488$ nm) in MDA-MB-231 cells was very similar (Fig. 17 c_{1,2}, d_{1,2}). After 3, 6 and 24 hours of incubation 68.8 %, 70.0 % and 74.6 % of cells had internalized BSA-Au NCs. For comparison, 89.4 %, 99 % and 100 % of MDA-MB-231 cancer cells had internalized BSA-Alexa 488 conjugate after 3, 6 and 24 hours of incubation respectively (Fig. 17 A). Mean photoluminescence intensity (MPI) values of BSA-Au NCs and BSA-Alexa conjugate per cell were also analyzed. The results have shown that MPI of the internalized BSA-Au NCs per cell does not increase over time in comparison with MPI after 3h of incubation in both MCF-7 and MDA-MB-231 cells (Fig. 18 B). On the contrary, MPI of the BSA-Alexa conjugate per cell after 6 and 24 h of incubation increased respectively 1.5 and 3.9 times in comparison with MPI after 3 h of incubation in MCF-7 cells. The difference was even higher for MDA-MB-231 cancer cells – the MPI of the BSA-Alexa conjugate per cell increased over time 1.9 and 7.3 times after 6 and 24 h of incubation respectively.

One of the reasons of significant differences in accumulation of BSA-Au NCs and BSA-Alexa conjugate measured using flow cytometry could be due to the modification of the secondary structure of the BSA after labelling [37], as previously it was shown that the size of BSA-Au NCs increased by approximately 2.5 nm compared to pure BSA. However, both BSA-Au NCs and BSA-Alexa conjugates were observed accumulated in vesicles at the perinuclear region (Fig. 17) indicating endocytotic uptake mechanism. Many authors have shown that BSA accumulates in cells via clathrin-mediated endocytosis and/or macropinocytosis [53-55].

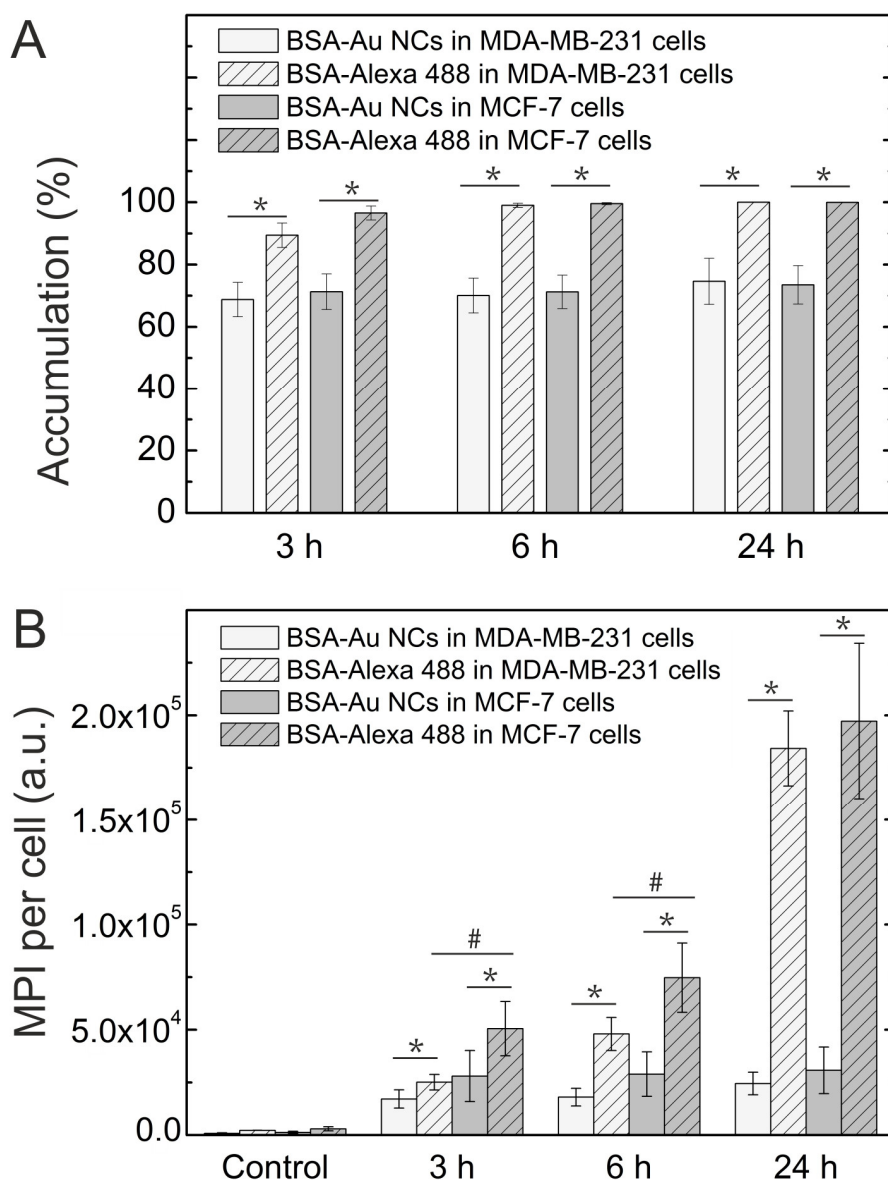


Fig. 18 Accumulation of photoluminescent BSA-Au NCs and BSA-Alexa conjugate in MCF-7 and MDA-MB-231 cells after 3, 6 and 24 h of incubation. Percentage of the cells that have accumulated BSA-Au NCs and BSA-Alexa conjugate (A); mean PL intensity (MPI) of BSA-Au NCs and BSA-Alexa conjugate per cell (B). Control represents autofluorescence of non-treated cells. Error bars show the standard deviations. * show significant differences between accumulation of BSA-Alexa 488 and BSA-Au NCs ($p \leq 0.05$); # show significant differences between the MCF-7 and MDA-MB-231 cell lines ($p \leq 0.05$)

Accumulation of photoluminescent Au-MES NCs was very different from accumulation of BSA-Au NCs. After 3 hours of incubation with Au-MES NCs solution MCF-7 cells exhibited homogeneously distributed green photoluminescence ($\lambda_{\text{ex}} = 405 \text{ nm}$) in 450-500 nm spectral region that was not observed in control group, only a few non-viable cells were stained with propidium iodide (Fig. 19). After 6 hours of incubation the PL intensity inside the cells was higher, however, more of the cells were stained with propidium iodide indicating increased cytotoxic effect. After 24 hours of incubation the photoluminescence intensity increased even more, however, the propidium iodide staining revealed that almost all of the MCF-7 cells were non-viable. Simultaneous decrease of total number of the cells showed high cytotoxicity of Au-MES NCs solution.

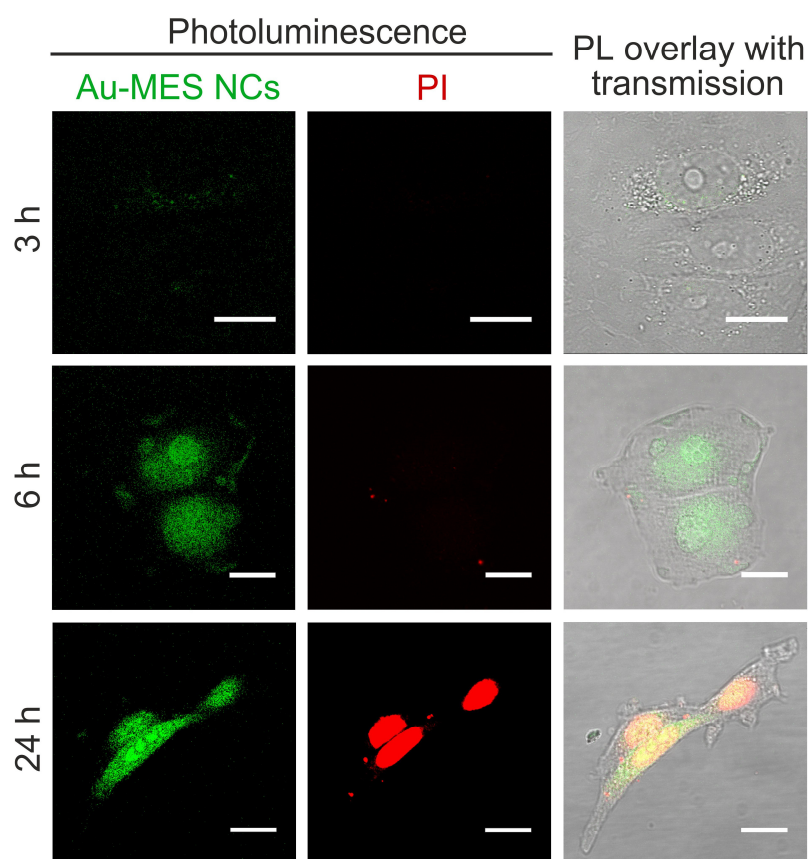


Fig. 19 Accumulation of photoluminescent Au-MES NCs ($\lambda_{\text{ex}} = 405 \text{ nm}$) in MCF-7 breast cancer cells after 3, 6 and 24 h of incubation (green photoluminescence). Red fluorescence represents propidium iodide stained non-viable cells ($\lambda_{\text{ex}} = 488 \text{ nm}$). Yellow colour in the merged pictures presents overlap of photoluminescence of Au-MES NCs and fluorescence of propidium iodide. Scale bar is $15 \mu\text{m}$

Accumulation of photoluminescent Au-MES NCs in MDA-MB-231 cells was very similar (Fig. 20 c_{1,2}) the PL was distributed homogeneously throughout the whole cell volume

including cell nucleus while both BSA-Alexa 488 conjugate and photoluminescent BSA-Au NCs were accumulated in vesicles at the perinuclear region (Fig. 20 a_{1,2}, b_{1,2}).

It is known that some small, hydrophilic organic molecules, like sugars, can pass through the cell membrane by facilitated diffusion. There are several reports showing that gold nanoparticles, smaller than 1.4 nm in diameter can also pass through the cell membrane and even through nuclear membrane diffusely [56]. Previously it was calculated that synthesized photoluminescent Au-MES NCs consist of ~9-10 gold atoms showing that the size of the nanoclusters should be below 0.5 nm in diameter. Therefore, the small size of Au-MES NCs allows them to pass through the cell membrane and even through nuclear membrane diffusely.

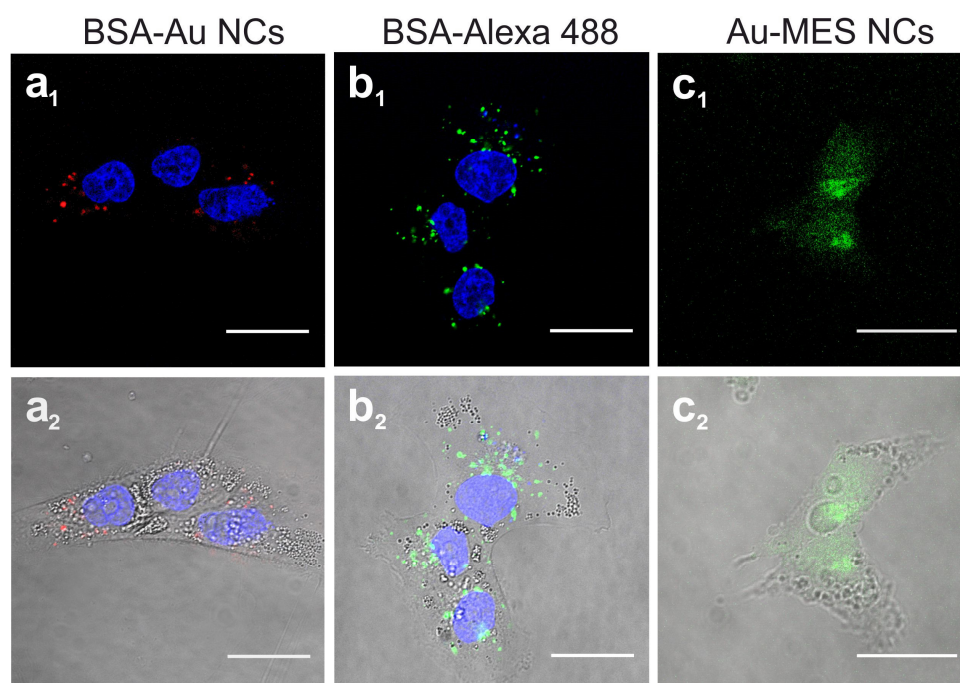


Fig. 20 Accumulation of photoluminescent BSA-Au NCs ($\lambda_{\text{ex}} = 488 \text{ nm}$), BSA-Alexa 488 conjugate ($\lambda_{\text{ex}} = 488 \text{ nm}$) and photoluminescent Au-MES NCs in MDA-MB-231 cells. Cells were incubated with BSA-Au NCs and BSA-Alexa 488 conjugate for 24 h, with Au-MES NCs – for 6 h. In a_{1,2} and b_{1,2} nuclei were stained with Hoechst 33258 ($\lambda_{\text{ex}} = 405 \text{ nm}$). Scale bar is 25 μm

3.5. Cytotoxicity of Au NCs

To investigate the cytotoxicity of BSA-Au NCs and Au-MES NCs, cell viability upon exposure to these Au NCs were examined using ADAM-MC Automatic Cell Counter. As it is presented in Fig. 21, cytotoxicity results showed no significant statistical difference of influence of BSA-Au NCs on viability of MCF-7 and MDA-MB-231 cells after

24 hours of incubation. Incubation with BSA solution also did not affect cell viability. Cytotoxicity assessments by other authors found BSA-Au NCs to be non-toxic to several other cell lines [57-60]. In contrast, 24 hours incubation time was lethal in case of incubation with Au-MES NCs – cell viability of only 13.8 % and 19.5 % was calculated for MCF-7 and MDA-MB-231 cells respectively (Fig. 21). However, at shorter incubation times Au-MES NCs exhibited lower cytotoxicity: after 3 hours of incubation with Au-MES NCs cell viability of MCF-7 and MDA-MB-231 cells was 78.1 % and 93.1 % respectively, after 6 h of incubation – 50.9 % and 80.7 %. The cytotoxic effect of MES solution (1 M, pH 6.3) after 24 hours of incubation was quite low, the cell viability of MCF-7 and MDA-MB-231 cells decreased to 86.1 % and 93.6 % respectively.

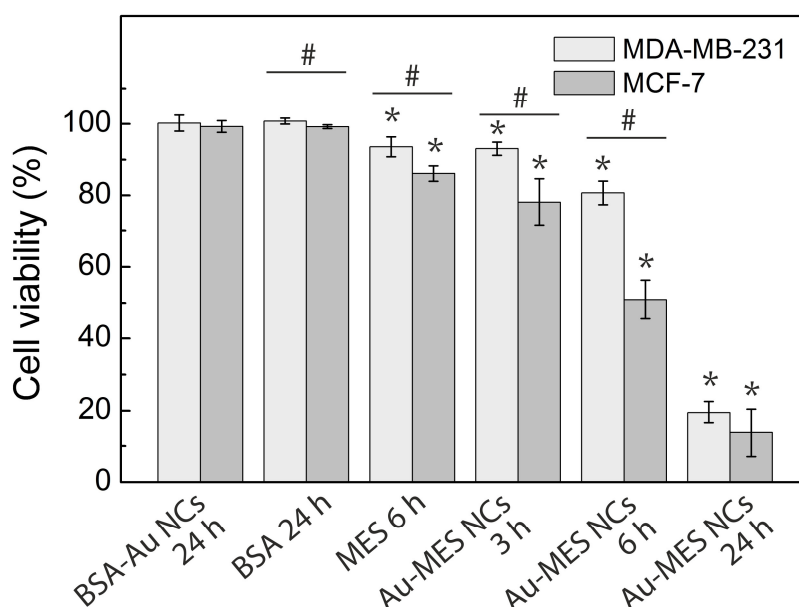


Fig. 21 Cell viability of MCF-7 and MDA-MB-231 cells incubated with BSA-Au NCs, BSA, Au-MES NCs and MES solutions. Error bars show the standard deviations. * Show significant differences compared to the non-treated cells ($p \leq 0.05$); # show significant differences between the MCF-7 and MDA-MB-231 cell lines ($p \leq 0.05$)

There are quite a few reports showing that smaller nanoparticles exhibit higher toxicity [61-63]. Other components of the synthesis such as MES have shown low toxicity in high doses (Fig. 21), HAuCl_4 has also been reported to be not toxic in low doses [64]. However, it is difficult to evaluate the cytotoxicity of photoluminescent Au-MES NCs alone, as it is known that during the synthesis larger, up to 10 nm in size, non-luminescent, yet non-plasmonic nanoparticles are formed.

3.6. ROS generation of Au NCs in cancer cells

In order to determine whether generation of reactive oxygen species (ROS) caused by interaction of cells with Au-MES NCs plays a role in cell death induction, we used a flow cytometry assay to detect ROS in live cells. In this study cells were treated with Au-MES NCs and BSA-Au NCs with following incubation with CellROX Green fluorescent ROS dye. Cells treated with 400 $\mu\text{g}/\text{mL}$ of TBHP and CellROX Green were taken as positive control, and cells treated only with fluorescent ROS dye represent negative control. The results showed that treatment with Au-MES NCs significantly increased intracellular ROS production (Fig. 7). After 3 and 6 hours of treatment ROS generation in MDA-MB-231 cancer cells has increased by 36.5 and 75.6 % respectively in comparison with negative control. The effect on MCF-7 cancer cells was even higher – after 3 and 6 hours of treatment with Au-MES NCs ROS generation has increased by 64.7 % and 118.2 % respectively in comparison with negative control. Incubation with MES solution (0.25 M) for 24 hours induced increase in ROS production by 68.7 % and 89.2 % in MDA-MB-231 and MCF-7 cells respectively. ROS production in the MDA-MB-231 cells treated with BSA-Au NCs for 24 hours was not significantly different from the negative control, however, in MCF-7 cells ROS generation has increased by 40.1 % in comparison with the negative control. Similar results were obtained as the cells were incubated with BSA solution – ROS generation increased by 19.8 % in MDA-MB-231, yet was not significantly different from negative control, meanwhile in MCF-7 cells ROS generation increased by 46.2 %.

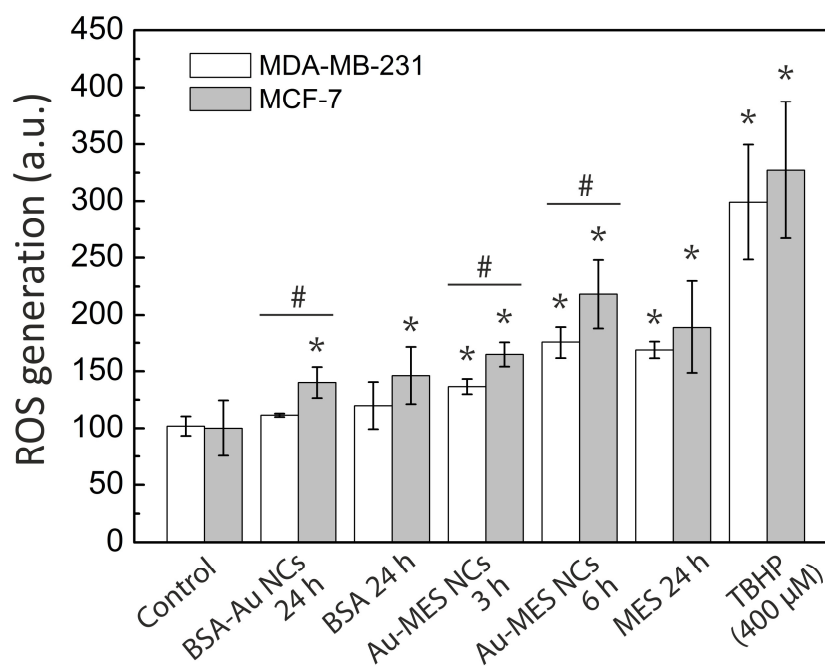


Fig. 22 ROS generation in MCF-7 and MDA-MB-231 cancer cells after treatment with BSA-Au NCs, Au-MES NCs, BSA and MES. The data normalized according to the ROS generation of the non-treated cells (Control). Error bars show the standard deviations. * Show significant differences compared to the non-treated cells ($p \leq 0.05$); # show significant differences between the MCF-7 and MDA-MB-231 cell lines ($p \leq 0.05$)

Only negligible increase in intracellular ROS generation induced by treatment with protein-encapsulated Au NCs have been reported by other authors [59] showing that proteins serve as remarkable coating in terms of biocompatibility. On the contrary, presumably due to ultrasmall size leading to a more widespread intracellular distribution including cell nuclei, Au-MES NCs were found more biologically reactive than BSA-Au NCs. Such exposure increased the possibility of Au-MES NCs interaction with vital cell components, including cell DNA, therefore, the toxicity (Fig. 21) along with generation of ROS (Fig. 22) has increased greatly over time. The generation of ROS induced by nanomaterials can contribute to number of biological stress responses and impair basic cellular functions leading to cell cycle arrest or even apoptosis [65, 66].

The cytotoxic effect of Au-MES NCs was more significant on MCF-7 cells than on MDA-MB-231 cells, along with higher intracellular ROS generation, showing that MDA-MB-231 cells are more resistant to treatment and exhibit properties of cancer stem-like cells [67, 68].

4. CONCLUSIONS

1. Synthesized BSA-encapsulated Au NCs were composed of 29 gold atoms on average and exhibited photoluminescence in spectral region of tissue optical window at 600-700 nm, therefore, they could be used for cancer fluorescence imaging. Meanwhile, photoluminescent Au-MES NCs were composed of 9 gold atoms on average and exhibited photoluminescence in blue spectral region, therefore could be applicable for *in vitro* imaging.
2. Photoluminescent BSA-Au NCs are not stable under irradiation with UV/blue light. The shift of the photoluminescence spectrum to the shorter wavelength region shows irradiation-wavelength dependent degradation of Au NCs. Under irradiation with 405 nm wavelength light, gold nanocluster loses 1-2 gold atoms, while under irradiation with 280 nm, 3-4 atoms are lost.
3. Photoluminescent Au-MES NCs are not stable under irradiation with UV/blue light. Under irradiation with 405 nm wavelength light Au-MES NCs, exhibiting photoluminescence at 476 nm degrade and smaller photoluminescent Au-MES NCs ($\lambda_{em} = 430$ nm) are formed.
4. Photoluminescent Au-MES NCs distributed diffusely in MCF-7 and MDA-MB-231 cells including cell nuclei possibly due to ultrasmall size. This led to increased cytotoxicity and intracellular generation of reactive oxygen species in cancer cells. Therefore, Au-MES NCs are not suitable for cancer fluorescence imaging.
5. Photoluminescent BSA-Au NCs accumulated in vesicles at the perinuclear region in MCF-7 and MDA-MB-231 cells and did not induce significant cytotoxic effect, therefore after further investigations *in vivo*, could be used for cancer fluorescence imaging.

5. SANTRAUKA (Summary in Lithuanian)

Įvadas

Onkologiniai susirgimai – dažniausia mirties priežastis ekonomiškai išsivysčiusiose šalyse bei pasauliniu mastu. Pasaulinės sveikatos organizacijos (angl. *World Health Organization*) statistikos duomenimis, 2012 metais pasaulyje diagnozuota ~14 mln. naujų vėžinių susirgimų atvejų. Prognozuojama, kad per artimiausius dvidešimt metų šis skaičius išaugs dar 70 % – t.y. kasmet bus diagnozuojama ~25 mln. naujų atvejų [1]. Mažėjant vidutiniam onkologinių pacientų amžiui, stipriai išauga vėžinių susirgimų keliami ekonominė našta valstybėms. Siekiant padidinti pacientų išgyvenamumo rodiklius bei pagerinti jų gyvenimo kokybę būtina tobulinti ankstyvos diagnostikos metodus ir ieškoti efektyvesnių terapijos būdų.

Viena iš geriausiai vertinamų ateities biomedicinos technologijų, nanomedicina, pasitelkia itin mažo dydžio ir unikalių savybių nanodaleles ankstyvų stadijų onkologinių susirgimų diagnostikai bei terapijai. Mažo dydžio, biosuderinamos, fotostabilumu bei unikaliomis optinėmis ir magnetinėmis savybėmis pasižyminčios nanodalelės yra potencialūs kontrastiniai žymenys, vaistų nešikliai bei terapinės medžiagos biomedicinoje [2, 3]. Pastaruoju metu dėl mažo toksiškumo bei palyginti lengvai modifikuojamo paviršiaus sudarant jungtis su antikūnais, biožymenimis bei funkcinėmis molekulėmis ypač daug dėmesio susilaukė tauriųjų metalų (aukso, sidabro) nanodalelės [4]. Aukso nanodalelės gali būti taikomos kaip rentgenografiniai žymenys diagnostikoje bei vaizdinime, kaip termo-pažaidas sukeliančios medžiagos onkologinių ligų termoterapijoje [2, 5].

Fotoluminescuojantys molekuliniai aukso ir sidabro nanoklasteriai – nauja klasė koloidinių fotoluminescuojančių nanodarinių [6], ypač patrauklių biomedicininei terapijai ir diagnostikai bei biologiniams tyrimams [18, 19].

Biomedicininės diagnostikos ir terapijos srityje ypač svarbios nanodalelių optinės bei erdvinės savybės, sąveika su gyvu organizmu – nuo to priklauso nanodalelių kaip diagnostinių ir terapinių medžiagų efektyvumas bei pritaikymo biomedicinėje praktikoje galimybės.

Visgi, nepaisant didelės pažangos Au nanodalelių sintezės srityje, molekulinų fotoluminescuojančių Au nanoklasterių fotostabilumas bei sąveikos su ląstelėmis mechanizmai nėra išsamiai ištirti.

Darbo tikslas ir uždaviniai

Darbo tikslas:

Ištirti fotoluminescuojančių Au-MES bei Au-JSA nanoklasterių pritaikymo galimybes fluorescencinei vėžio diagnostikai.

Uždaviniai:

1. Ištirti Au-MES bei Au-JSA nanoklasterių struktūrą bei spektrines savybes.
2. Ištirti Au-MES bei Au-JSA nanoklasterių stabilumą švitinant UV/Vis spinduliuote.
3. Palyginti Au-MES bei Au-JSA nanoklasterių susikaupimą krūties vėžinėse ląstelėse.
4. Palyginti Au-MES bei Au-JSA nanoklasterių poveikį krūties vėžinių ląstelių gyvybingumui.
5. Palyginti Au-MES bei Au-JSA nanoklasterių poveikį krūties vėžinių ląstelių reaktyvių deguonies formų generacijai.

Aktualumas ir naujumas

Kasmet sparčiai augantis naujų onkologinių susirgimų skaičius tiek Lietuvoje, tiek visame pasaulyje skatina įvairių sričių mokslininkus susivienyti bendram tikslui: ieškoma naujų efektyvesnių ankstyvos onkologinių ligų diagnostikos priemonių.

Vis daugiau biomedicinos diagnostikos technologijų pasitelkia optinę diagnostiką. Optinės diagnostikos technologijos plačiai taikomos biomedicinoje atliekant tyrimus spektroskopiniais, tėkmės citometrijos, klinikinės chemijos, imunologiniais metodais bei naudojant įvairius biojutiklius, ir netgi chirurgijoje [7-11]. Tokių technologijų pagrindas – fluorescenciniai žymenys.

Mažos molekulinės masės fluorescuojančios organinės molekulės buvo pirmieji ir plačiausiai fluorescencinėje diagnostikoje taikomi žymenys. Jie pasižymi dideliu kvantiniu našumu bei yra lengvai konjuguojami su specifinėmis molekulėmis, taip pat – pigūs [12]. Visgi, nors organiniai fluorescenciniai žymenys vis dar plačiai naudojami biomolekulėms vaizdinti, jų taikymą audinių vaizdinimui *in vivo* ir tolimesniuose klinikiniuose tyrimuose riboja prastas fotostabilumas [13, 14].

Fotostabilumas – vienas pagrindinių kokybinių fluorescencinių žymenų parametrų, kadangi UV/Vis spinduliuotė yra naudojama sužadinti žymenų fluorescencijai. Net ir mažo intensyvumo nuolatinė spinduliuotė gali turėti įtakos fluorescencijos blyškimui (angl. *photo-bleaching*) bei fluorescencinio žymens irimui (angl. *photo-degradation*), o pastarasis gali turėti lemiamos įtakos fluorescuojančių žymenų toksiškumui. Ieškant naujų, geresnėmis optinėmis savybėmis pasižyminčių fluorescencinių žymenų, mokslininkų ir medikų dėmesys nukrypo į pastarąjį dešimtmetį itin sparčiai besivystančias nanotechnologijas. Itin mažo dydžio ir unikaliomis savybėmis pasižyminčios nanodalelės skiriasi keliais būdais: į biomediciną [2, 15]. Jau kurį laiką intensyviai tyrinėjamos fotoluminescuojančios puslaidininkinės nanodalelės – kvantiniai taškai – fotoluminescencijos kvantiniu našumu neatsilieka, o fotostabilumu ženkliai lenkia organinius fluorescencinius žymenis [16], tačiau šios puslaidininkinės nanodalelės yra sudarytos iš toksinių cheminių elementų, o dėl stabilizuojančių sluoksnių bei sąveikos su kraujo plazmos baltymais išaugęs nanodalelių dydis apsunkina jų pašalinimą iš organizmo per inkstų kanalus [17]. Todėl ankstyvaisiais 2000 metais susintetinus pirmuosius vandenyje tirpius fotoluminescuojančius tauriųjų metalų nanoklasterius [6], visų mokslininkų dėmesys nukrypo į juos.

Fotoluminescuojantys, į molekulių panašiomis savybėmis pasižymintys aukso ir sidabro nanoklasteriai yra nauja klasė koloidinių fotoluminescuojančių nanodarinių, ypač patrauklių medicininei terapijai ir diagnostikai bei biologiniams tyrimams [18, 19]. Efektyviam fotoluminescuojančių Au NK taikymui fluorescenciniam vaizdinimui labai svarbus jų optinių savybių stabilumas. Fotoluminescuojantys Au NK dažnai minimi kaip nanodariniai, pasižymintys dideliu stabilumu, tačiau duomenų apie Au NK fotostabilumą nėra daug [20-25]. Literatūroje yra parodyta, jog fotoluminescuojantys Au NK gali pasižymėti fotostabilumu, juos švitinant UV/Vis spinduliuote [20-22], tačiau yra duomenų ir apie Au NK, kurie, veikiami UV/Vis spinduliuote, blykšta [23-25]. Visgi dauguma autorių, pateikdami fotostabilumo tyrimų duomenys, pateikia tik FL intensyvumą, nenagrinėdami spektro formos pokyčių, taip išvengdami diskusijų dėl šviesos poveikio nanoklasterio paviršiaus dangalui ar net pačiam nanoklasterio dydžiui, taigi Au NK fotostabilumas bei galimi jo mechanizmai nėra išsamiai ištirti.

Nepaisant itin didelio susidomėjimo Au NK pritaikymu biomedicinoje, fotoluminescuojančių Au NK susikaupimas ląstelėse bei poveikis jų gyvybiniam procesams nėra išsamiai ištirtas. Literatūros duomenys yra gana kontroversiški, rodantys, jog Au NK susikaupimas bei pasiskirstymas ląstelėse labai priklauso nuo Au NK dydžio, paviršiaus dangalo molekulių, krūvio ir t.t. [26, 27].

Šiame darbe pirmą kartą ištirtas fotoluminescuojančių jaučio serumo albumino baltyme susintetintų aukso nanoklasterių bei 2-(N-morfolino) etanesulfonine rūgštimi dengtų fotoluminescuojančių aukso nanoklasterių fotostabilumas, palygintas šių fotoluminescuojančių aukso nanoklasterių susikaupimas dviejose skirtingo piktybiškumo bei invazyvumo krūties vėžio ląstelėse (MCF-7 ir MDA-MB-231 ląstelių linijose), ištirtas jų poveikis šių ląstelių gyvybingumui bei aukso nanoklasterių indukuota aktyvių deguonies formų generacija ląstelėse.

Ginamieji teiginiai

1. Atlikus aukso nanoklasterių spektrinių charakteristikų bei erdvinių savybių matavimus bei pasitelkus laisvųjų elektronų dujų modelį nustatyta, kad fotoluminescuojančių jaučio serumo albumine (JSA) susintetintų aukso nanoklasterių skersmuo yra ne didesnis nei 1,3 nm, ir jį sudaro vidutiniškai 29 aukso atomai, tuo tarpu 2-(N-morfolino) etanesulfonine rūgštimi (MES) dengti fotoluminescuojantys aukso nanoklasteriai yra ne didesni nei 0,5 nm, ir sudaryti iš vidutiniškai 9 aukso atomų.
2. UV/mėlynos šviesos poveikyje keičiasi Au-JSA NK bei Au-MES NK spektrinės savybės, kurios rodo, kad šviesos poveikyje fotoluminescuojantys Au NK yra. Au-JSA NK irimas priklauso nuo švitinimo bangos ilgio: kai $\lambda = 405$ nm, prarandami 1-2 aukso atomai, kai $\lambda = 280$ nm – 3-4 atomai; veikiant $\lambda = 405$ nm spinduliuote, Au-MES NK dydis sumažėja 1-2 atomais.
3. Fotoluminescuojantys Au-JSA NK ir Au-MES NK kaupiasi ląstelėse: mažesnio dydžio Au-MES NK vėžinėse ląstelėse pasiskirsto difuziškai citoplazmoje ir ląstelių branduoliuose, tuo tarpu Au-JSA NK lokalizuoti pūslelių tipo dariniuose ląstelių citoplazmoje ir nepatenka į branduolius.
4. 24 val. inkubacija Au-JSA NK neturi įtakos vėžinių ląstelių gyvybingumui, tuo tarpu Au-MES NK pasižymi nuo inkubacijos trukmės priklausomu toksiškumu vėžinėms ląstelėms.
5. Au-MES NK inkubuotose vėžinėse ląstelėse išauga aktyvių deguonies formų generacija, tuo tarpu Au-JSA NK nesukėlė aktyvių deguonies formų generacijos pokyčio MDA-MB-231 ląstelėse.

Pagrindiniai rezultatai

Šiame darbe nagrinėjamos fotoluminescuojančių Au-JSA bei Au-MES nanoklasterių optinės ir erdvinės savybės bei biologinis suderinamumas siekiant įvertinti nanoklasterių pritaikymo fluorescencinei diagnostikai biomedicinoje galimybes.

Optinės savybės ir jų stabilumas lemia, ar fluorescenciniai žymenys yra tinkami biomediciniam vaizdinimui: ar jų susikaupimą bei pasiskirstymą ląstelėse ir audiniuose galima įvertinti neinvaziniais optiniais metodais. Nuostoviosios spektroskopijos metodais išmatavus susintetintų Au-JSA NK spektrines charakteristikas nustatyta, jog Au-JSA NK fotoluminescuoja raudonoje spektrinėje srityje 600-700 nm, ir pasižymi plačiu FL žadinimo spektru (5 pav.). Tuo tarpu susintetinti Au-MES NK pasižymėjo fotoluminescencija mėlynoje spektrinėje srityje ties 476 nm (6 pav.).

Aukso nanoklasterių erdvinės charakteristikos turi didelės įtakos jų susikaupimui bei pasiskirstymui ląstelėse ir audiniuose. Palyginus ant žėručio paviršiaus paskleistų Au-JSA NK bei JSA atomo jėgos mikroskopijos rezultatus nustatyta, jog jaučio serumo albumine susiformavę Au NK yra mažesnis nei 1,3 nm (7 pav.), o pasitelkus laisvųjų elektronų dujų modelį apskaičiuota, jog Au-JSA nanoklasteriai yra sudaryti iš vidutiniškai 29 aukso atomų.

Atlikus nuostoviosios sugerties ir fluorescencijos matavimus nustatyta, jog Au-MES ND koloidinis tirpalas nėra homogeniškas jį sudaro fotoluminescuojantys Au NK bei nefotoluminescuojančios Au-MES ND. Tą patvirtino atomo jėgos mikroskopijos bei elektronų pralaidumo mikroskopijos matavimų rezultatai – nustatyta, jog koloidinį Au-MES ND tirpalą sudaro 0,5-10 nm dydžio nanodalelės (10 pav.). Tuo tarpu pasitelkus laisvųjų elektronų dujų modelį nustatyta, kad fotoluminescuojantys Au-MES NK ($FL \lambda_{\max} = 660 \text{ nm}$), sudaryti iš vidutiniškai 9 aukso atomų.

Efektyviam fotoluminescuojančių Au NK taikymui biomedicinoje labai svarbus jų optinių savybių stabilumas veikiant žadinančia UV/Vis spinduliuote. Atlikus fotostabilumo tyrimus nustatyta, jog UV/mėlyna spinduliuotė sukelia stiprius ir nuo švitinimo bangos ilgio priklausomus Au-JSA NK fotoluminescencijos spektro pokyčius (11 pav.). Apskaičiuota, jog Au-JSA NK veikiant 405 nm bei 492 nm spinduliuote išmatuotas 6-10 nm hipsochrominis FL juostos poslinkis atitiktų nanoklasterio sumažėjimą vienu-dviem aukso atomais. Tuo tarpu švitinant Au-JSA nanoklasterius 280 nm spinduliuote nanoklasteriai

sumažėja net 3-4 atomais. Visgi galima ir kita FL juostos intensyvumo mažėjimo bei hipsochrominio poslinkio priežastis švitinant Au-JSA NK – tai nanoklasterių paviršiaus dangalo (JSA) pažeidimas.

Poveikis UV/mėlyna spinduliuote sukėlė stiprius ir nuo švitinimo bangos ilgio priklausomus pokyčius ir Au-MES NK sugerties bei fotoluminescencijos spektruose. Švitinant 402 nm spinduliuote mažėjo Au-MES NK fotoluminescencijos spektro smailės ties 476 nm ($\lambda_{\text{žad.}} = 405$ nm) intensyvumas, smailė slinkosi į trumpabangę pusę, ties 430 nm formavosi nauja FL juosta (13 pav.). Pasitelkus jau anksčiau aprašytą laisvųjų elektronų dujų modelį, buvo apskaičiuota, jog švitinimo 402 nm spinduliuote metu iš vidutiniškai 9 aukso atomų Au-MES NK formuojasi mažesni, iš vidutiniškai 7 aukso atomų sudaryti nanoklasteriai.

Fotoluminescuojančių aukso nanoklasterių biosuderinamumas buvo įvertintas ištyrus jų susikaupimą bei poveikį dviejų skirtingo piktybiškumo bei invazyvumo krūties vėžio linių ląstelių (MCF-7 ir MDA-MB-231) gyvybingumui bei aktyvių deguonies formų generacijai. Fluorescencinės konfokalinės mikroskopijos metodu nustatyta, jog fotoluminescuojantys Au-JSA NK, ir JSA-Alexa 488 konjugatas MDA-MB-231 bei MCF-7 ląstelėse kaupiasi pūslelėse, išsidėsčiusiose palei branduolį. Ląstelių branduoliuose šių medžiagų susikaupimo nebuvo pastebėta (20 pav.).

Fotoluminescuojančių Au-MES NK susikaupimas ląstelėse labai skyrėsi nuo Au-JSA NK susikaupimo. Po 3 ir 6 h inkubacijos su Au-MES NK abiejų linių ląstelių ląstelėse pasižymėjo visame ląstelių tūryje tolygiai pasiskirsčiusia fotoluminescencija, registruojama ir ląstelės branduolyje bei patenkančia į 450-500 nm spektrinę sritį (19 pav.). Manoma, kad difuzinį pasiskirstymą nulėmė itin mažas Au-MES NK dydis.

Rezultatai parodė, jog Au-MES NK paveiktose ląstelėse žymiai išauga aktyvių deguonies formų generacija bei sumažėja gyvybingumas, tuo tarpu ląstelių inkubacija JSA bei Au-JSA NK nesukėlė poveikio ląstelių gyvybingumui (21, 22 pav.).

Apibendrinant galima teigti, kad itin maži, fotoluminescencija mėlynoje spektrinėje srityje pasižymintys Au-MES NK nėra tinkami biologinių objektų vaizdinimui, nes veikiant mažo intensyvumo UV/Vis spinduliuote yra nestabilūs, yra. Mažas šių nanoklasterių dydis lemia nespecifinį pasiskirstymą visame ląstelės tūryje įskaitant ląstelės branduolį, dėl ko

galimai išauga nanoklasterių sąveika su gyvybiškai svarbiais ląstelės komponentais, tokiomis kaip DNR, o kartu – citotoksinis poveikis bei aktyvių deguonies formų generacija. Tuo tarpu Au-JSA NK fotoluminescuoja raudonoje spektrinėje srityje, kur audinių optinė sugertis yra mažiausia („audinių optinio skaidrumo langas“), kaupiasi skirtingo invazyvumo vėžinėse ląstelėse bei yra netoksiški. todėl galėtų būti panaudoti fluorescenciniam navikų vaizdinimui. Visgi veikiami UV/Vis spinduliuote Au-JSA NK nėra stabilūs, ilgalaikė ekspozicija lemia nanoklasterių spektrinius ir struktūrinius pokyčius, todėl siekiant juos panaudoti biomedicininiam vaizdinimui reikėtų ištirti jų fototoksiškumą.

Viena iš Au NK spektrinių ir struktūrinių pokyčių priežasčių, juos veikiant UV/mėlyna spinduliuote, yra generuojamos aktyvios deguonies formos. Tęsiant tyrimus šioje srityje būtų galima įvertinti aukso nanoklasterių pritaikomumą ne tik fluorescencinėje diagnostikoje, bet ir fotosensibilizuotoje navikų terapijoje, pasitelkiančioje aktyvias deguonies formas sukelti navikinių ląstelių žūčiai.

Išvados

1. Au-JSA NK sintezės metu susiformuoja vidutiniškai 29 aukso atomų nanoklasteriai, kurie pasižymi fotoluminescencija audinių skaidrumo lango 600-700 nm spektrinėje srityje, todėl galėtų būti panaudoti navikinių darinių fluorescenciniam vaizdinimui. Tuo tarpu Au-MES NK sintezės metu susiformuoja maži, vidutiniškai 9 aukso atomų dydžio mėlynoje spektrinėje srityje fotoluminescuojantys nanoklasteriai, tinkami tyrimams *in vitro*.
2. UV/mėlynos šviesos poveikyje fotoluminescuojantys Au-JSA NK yra nestabilūs, stebimas jų fotoluminescencijos spektro poslinkis į trumpųjų bangų spektrinę sritį. Au-JSA NK irimas priklauso nuo švitinimo bangos ilgio: veikiant $\lambda = 405$ nm spinduliuote, prarandami 1-2 aukso atomai, kai $\lambda_{\text{švit.}} = 280$ nm, prarandami 3-4 atomai.
3. UV/mėlynos šviesos poveikyje fotoluminescuojantys Au-MES NK yra nestabilūs. Veikiant 405 nm spinduliuote, Au-MES NK, fotoluminescuojantys ties 476 nm, yra, iš jų formuojasi mažesni, ties 430 nm fotoluminescuojantys Au-MES NK, sudaryti iš vidutiniškai 7 aukso atomų.
4. Mažo dydžio, difuziškai vėžinių ląstelių citoplazmoje ir branduoliuose pasiskirstę Au-MES NK pasižymėjo nuo inkubacijos trukmės priklausomu toksiškumu bei išaugusia aktyvių deguonies formų generacija ląstelėse, todėl nėra tinkami fluorescencinės diagnostikos tyrimams.
5. Susikaupę pūslelėse išsidėsčiusiose palei branduolį Au-JSA NK nesukėlė toksinio poveikio vėžinėms ląstelėms, nors MCF-7 ląstelėse lėmė išaugusią aktyvių deguonies formų generaciją, todėl atlikus tolimesnius tyrimus *in vivo* galėtų būti pritaikyti fluorescenciniam navikų vaizdinimui.

ACKNOWLEDGEMENT

Foremost, I would like to express sincere gratitude to my supervisor prof. Ričardas Rotomskis for the valuable discussions, advices and support during the doctoral studies.

I would like to thank Department of Quantum Electronics for advices and help.

I am grateful to Dominyka Dapkutė, Greta Jarockytė and Laima Budėnaitė for the help with experiments *in vitro*.

I would like to express the deepest appreciation to the team members of Biomedical Physics Laboratory for the comprehension, advices and support. I could not have imagined having better colleagues.

I would like to thank my family and friends, especially my parents for supporting me spiritually throughout writing this thesis.

6. REFERENCES

1. World cancer report 2014, B.W. Stewart and C.P. Wild, Editors. International Agency for Research on Cancer: Lyon, France (2014).
2. E.-K. Lim, T. Kim, S. Paik, S. Haam, Y.-M. Huh, and K. Lee, Nanomaterials for theranostics: Recent advances and future challenges, *Chem. Rev.*, **115**(1), 327-394 (2015).
3. N. Bertrand, J. Wu, X. Xu, N. Kamaly, and O.C. Farokhzad, Cancer nanotechnology: The impact of passive and active targeting in the era of modern cancer biology, *Adv. Drug Deliv. Rev.*, **66**, 2-25 (2014).
4. L. Dykman and N. Khlebtsov, Gold nanoparticles in biomedical applications: Recent advances and perspectives, *Chem. Soc. Rev.*, **41**(6), 2256-2282 (2012).
5. J. Lin, S. Wang, P. Huang, Z. Wang, S. Chen, G. Niu, W. Li, J. He, D. Cui, G. Lu, et al., Photosensitizer-loaded gold vesicles with strong plasmonic coupling effect for imaging-guided photothermal/photodynamic therapy, *ACS Nano*, **7**(6), 5320-5329 (2013).
6. J. Zheng, C.W. Zhang, and R.M. Dickson, Highly fluorescent, water-soluble, size-tunable gold quantum dots, *Phys. Rev. Lett.*, **93**(7), 077402 (2004).
7. R. Weissleder and M.J. Pittet, Imaging in the era of molecular oncology, *Nature*, **452**(7187), 580-589 (2008).
8. S.M. Borisov and O.S. Wolfbeis, Optical Biosensors, *Chem. Rev.*, **108**(2), 423-461 (2008).
9. L. Xi and H. Jiang, Image-guided surgery using multimodality strategy and molecular probes, *WIREs Nanomed. Nanobiol.*, **8**(1), 46-60 (2016).
10. J.R.W. Conway, N.O. Carragher, and P. Timpson, Developments in preclinical cancer imaging: Innovating the discovery of therapeutics, *Nat. Rev. Cancer*, **14**(5), 314-328 (2014).
11. A.L. Vahrmeijer, M. Hutteman, J.R. van der Vorst, C.J.H. van de Velde, and J.V. Frangioni, Image-guided cancer surgery using near-infrared fluorescence, *Nat. Rev. Clin. Oncol.*, **10**(9), 507-518 (2013).
12. A. Gust, A. Zander, A. Gietl, P. Holzmeister, S. Schulz, B. Lalkens, P. Tinnefeld, and D. Grohmann, A starting point for fluorescence-based single-molecule measurements in biomolecular research, *Molecules*, **19**(10), 15824 (2014).
13. N. Panchuk-Voloshina, R.P. Haugland, J. Bishop-Stewart, M.K. Bhalgat, P.J. Millard, F. Mao, W.Y. Leung, and R.P. Haugland, Alexa dyes, a series of new fluorescent dyes that yield exceptionally bright, photostable conjugates, *J. Histochem. Cytochem.*, **47**(9), 1179-1188 (1999).

14. J.E. Berlier, A. Rothe, G. Buller, J. Bradford, D.R. Gray, B.J. Filanoski, W.G. Telford, S. Yue, J. Liu, C.-Y. Cheung, et al., Quantitative comparison of long-wavelength Alexa Fluor dyes to Cy dyes: Fluorescence of the dyes and their bioconjugates, *J. Histochem. Cytochem.*, **51**(12), 1699-1712 (2003).
15. R. Weissleder, M. Nahrendorf, and M.J. Pittet, Imaging macrophages with nanoparticles, *Nat. Mater.*, **13**(2), 125-138 (2014).
16. U. Resch-Genger, M. Grabolle, S. Cavaliere-Jaricot, R. Nitschke, and T. Nann, Quantum dots versus organic dyes as fluorescent labels, *Nat. Meth.*, **5**(9), 763-775 (2008).
17. H. Soo Choi, W. Liu, P. Misra, E. Tanaka, J.P. Zimmer, B. Itty Ipe, M.G. Bawendi, and J.V. Frangioni, Renal clearance of quantum dots, *Nat. Biotech.*, **25**(10), 1165-1170 (2007).
18. C.A.J. Lin, C.H. Lee, J.T. Hsieh, H.H. Wang, J.K. Li, J.L. Shen, W.H. Chan, H.I. Yeh, and W.H. Chang, Synthesis of fluorescent metallic nanoclusters toward biomedical application: Recent progress and present challenges, *J. Med. Biol. Eng.*, **29**(6), 276-283 (2009).
19. S. Palmal and N.R. Jana, Gold nanoclusters with enhanced tunable fluorescence as bioimaging probes, *WIREs Nanomed. Nanobiol.*, **6**(1), 102-110 (2014).
20. C.T. Yuan, W.C. Chou, J. Tang, C.A. Lin, W.H. Chang, J.L. Shen, and D.S. Chuu, Single fluorescent gold nanoclusters, *Opt. Express*, **17**(18), 16111-16118 (2009).
21. Y.F. Kong, J. Chen, F. Gao, R. Brydson, B. Johnson, G. Heath, Y. Zhang, L. Wu, and D.J. Zhou, Near-infrared fluorescent ribonuclease-A-encapsulated gold nanoclusters: preparation, characterization, cancer targeting and imaging, *Nanoscale*, **5**(3), 1009-1017 (2013).
22. J. Sun, J. Zhang, and Y.D. Jin, 11-Mercaptoundecanoic acid directed one-pot synthesis of water-soluble fluorescent gold nanoclusters and their use as probes for sensitive and selective detection of Cr³⁺ and Cr⁶⁺, *J Mater Chem C*, **1**(1), 138-143 (2013).
23. C.A.J. Lin, T.Y. Yang, C.H. Lee, S.H. Huang, R.A. Sperling, M. Zanella, J.K. Li, J.L. Shen, H.H. Wang, H.I. Yeh, et al., Synthesis, characterization, and bioconjugation of fluorescent gold nanoclusters toward biological labeling applications, *ACS Nano*, **3**(2), 395-401 (2009).
24. H. Kawasaki, H. Yamamoto, H. Fujimori, R. Arakawa, Y. Iwasaki, and M. Inada, Stability of the DMF-protected Au nanoclusters: Photochemical, dispersion, and thermal properties, *Langmuir*, **26**(8), 5926-5933 (2010).

25. H. Kawasaki, K. Yoshimura, K. Hamaguchi, and R. Arakawa, Trypsin-stabilized fluorescent gold nanocluster for sensitive and selective Hg²⁺ detection, *Anal. Sci.*, **27**(6), 591-596 (2011).
26. A. Albanese, P.S. Tang, and W.C.W. Chan, The effect of nanoparticle size, shape, and surface chemistry on biological systems, *Annu. Rev. Biomed. Eng.*, **14**, 1-16 (2012).
27. L. Shang, K. Nienhaus, and G.U. Nienhaus, Engineered nanoparticles interacting with cells: size matters, *J. Nanobiotechnol.*, **12**(1), 1-5 (2014).
28. J.P. Xie, Y.G. Zheng, and J.Y. Ying, Protein-directed synthesis of highly fluorescent gold nanoclusters, *J. Am. Chem. Soc.*, **131**(3), 888-889 (2009).
29. V. Poderys, M. Matulionyte-Safine, D. Rupsys, and R. Rotomskis, Protein stabilized Au nanoclusters: Spectral properties and photostability, *Lith. J. Phys.*, **56**(1), 55-65 (2016).
30. Y.P. Bao, H.C. Yeh, C. Zhong, S.A. Ivanov, J.K. Sharma, M.L. Neidig, D.M. Vu, A.P. Shreve, R.B. Dyer, J.H. Werner, et al., Formation and stabilization of fluorescent gold nanoclusters using small molecules, *J. Phys. Chem. C*, **114**(38), 15879-15882 (2010).
31. 90Plus/BI-MAS multi angle particle sizing option operation manual, B. Inc.(1995).
32. V. Amendola and M. Meneghetti, Size evaluation of gold nanoparticles by UV-Vis spectroscopy, *J. Phys. Chem. C*, **113**(11), 4277-4285 (2009).
33. W. Haiss, N.T.K. Thanh, J. Aveyard, and D.G. Fernig, Determination of size and concentration of gold nanoparticles from UV-Vis spectra, *Anal. Chem.*, **79**(11), 4215-4221 (2007).
34. P.N. Njoki, I.I.S. Lim, D. Mott, H.Y. Park, B. Khan, S. Mishra, R. Sujakumar, J. Luo, and C.J. Zhong, Size correlation of optical and spectroscopic properties for gold nanoparticles, *J. Phys. Chem. C*, **111**(40), 14664-14669 (2007).
35. L.H. Jin, L. Shang, S.J. Guo, Y.X. Fang, D. Wen, L. Wang, J.Y. Yin, and S.J. Dong, Biomolecule-stabilized Au nanoclusters as a fluorescence probe for sensitive detection of glucose, *Biosens. Bioelectron.*, **26**(5), 1965-1969 (2011).
36. Z. Wu and R. Jin, On the ligand's role in the fluorescence of gold nanoclusters, *Nano Lett.*, **10**(7), 2568-73 (2010).
37. X. Le Guevel, B. Hotzer, G. Jung, K. Hollemeyer, V. Trouillet, and M. Schneider, Formation of fluorescent metal (Au, Ag) nanoclusters capped in bovine serum albumin followed by fluorescence and spectroscopy, *J. Phys. Chem. C* **115**(22), 10955–10963 (2011).
38. A.K. Wright and M.R. Thompson, Hydrodynamic structure of bovine serum albumin determined by transient electric birefringence, *Biophys. J.*, **15**(2 Pt 1), 137-41 (1975).

39. A.M. Moulin, S.J. O'Shea, R.A. Badley, P. Doyle, and M.E. Welland, Measuring surface-induced conformational changes in proteins, *Langmuir*, **15**(26), 8776-8779 (1999).
40. J.L. Brash and T.A. Horbett, *Proteins at Interfaces*, in *Proteins at interfaces II*. (American Chemical Society, 1995) pp. 1-23.
41. S. Demanèche, J.-P. Chapel, L.J. Monrozier, and H. Quiquampoix, Dissimilar pH-dependent adsorption features of bovine serum albumin and α -chymotrypsin on mica probed by AFM, *Colloids Surf. B Biointerfaces*, **70**(2), 226-231 (2009).
42. O. Mori and T. Imae, AFM investigation of the adsorption process of bovine serum albumin on mica, *Colloids Surf. B*, **9**(1), 31-36 (1997).
43. X.X. Wang, Y.Y. Wang, H.B. Rao, and Z. Shan, A sensitive fluorescent assay for trypsin activity in biological samples using BSA-Au nanoclusters, *J. Brazil. Chem. Soc.*, **23**(11), 2011-2015 (2012).
44. V. Poderys, M. Matulionyte, A. Selskis, and R. Rotomskis, Interaction of water-soluble CdTe quantum dots with bovine serum albumin, *Nanoscale Res. Lett.*, **6**(1), 1-6 (2011).
45. M. Matulionyte, R. Marcinonyte, and R. Rotomskis, Photoinduced spectral changes of photoluminescent gold nanoclusters, *J. Biomed. Opt.*, **20**(5), 051018 (2015).
46. W. Zhang, Y. Li, J. Niu, and Y. Chen, Photogeneration of reactive oxygen species on uncoated silver, gold, nickel, and silicon nanoparticles and their antibacterial effects, *Langmuir* **29**(15), 4647-4651 (2013).
47. M. Misawa and J. Takahashi, Generation of reactive oxygen species induced by gold nanoparticles under x-ray and UV Irradiations, *Nanomedicine*, **7**(5), 604-14 (2011).
48. H. Kawasaki, S. Kumar, G. Li, C.J. Zeng, D.R. Kauffman, J. Yoshimoto, Y. Iwasaki, and R.C. Jin, Generation of singlet oxygen by photoexcited Au₂₅(SR)₁₈ clusters, *Chem. Mater.*, **26**(9), 2777-2788 (2014).
49. A. Ramanavicius, V. Karabanovas, A. Ramanaviciene, and R. Rotomskis, Stabilization of (CdSe)ZnS quantum dots with polypyrrole formed by UV/VIS irradiation initiated polymerization, *J. Nanosci. Nanotechnol.*, **9**(3), 1909-1915 (2009).
50. E.A. Christensen, P. Kulatunga, and B.C. Lagerholm, A single molecule investigation of the photostability of quantum dots, *Plos One*, **7**(8), e0124852 (2012).
51. F. Aldeek, C. Mustin, L. Balan, G. Medjahdi, T. Roques-Carmes, P. Arnoux, and R. Schneider, Enhanced photostability from CdSe(S)/ZnO core/shell quantum dots and their use in biolabeling, *Eur. J. Inorg. Chem.*, (6), 794-801 (2011).
52. L.B. Zhang and E.K. Wang, Metal nanoclusters: New fluorescent probes for sensors and bioimaging, *Nano Today*, **9**(1), 132-157 (2014).

53. R. Yumoto, H. Nishikawa, M. Okamoto, H. Katayama, J. Nagai, and M. Takano, Clathrin-mediated endocytosis of FITC-albumin in alveolar type II epithelial cell line RLE-6TN, *Am. J. Physiol-Lung C*, **290**(5), L946-L955 (2006).
54. J. Eyre, K. Ioannou, B.D. Grubb, M.A. Saleem, P.W. Mathieson, N.J. Brunskill, E.I. Christensen, and P.S. Topham, Statin-sensitive endocytosis of albumin by glomerular podocytes, *Am. J. Physiol. Renal Physiol.*, **292**(2), F674-F681 (2007).
55. E. Dobrinskikh, K. Okamura, J.B. Kopp, R.B. Doctor, and J. Blaine, Human podocytes perform polarized, caveolae-dependent albumin endocytosis, *Am. J. Physiol. Renal Physiol.*, **306**(9), F941-F951 (2014).
56. H.Y. Chen, B.W. Li, C. Wang, X. Zhang, Z.Q. Cheng, X. Dai, R. Zhu, and Y.Q. Gu, Characterization of a fluorescence probe based on gold nanoclusters for cell and animal imaging, *Nanotechnology*, **24**(5), 055704 (2013).
57. H.Y. Chen, B.W. Li, X.Y. Ren, S.N. Li, Y.X. Ma, S.S. Cui, and Y.Q. Gu, Multifunctional near-infrared-emitting nano-conjugates based on gold clusters for tumor imaging and therapy, *Biomaterials*, **33**(33), 8461-8476 (2012).
58. H.Y. Chen, S.L. Li, B.W. Li, X.Y. Ren, S.N. Li, D.M. Mahounga, S.S. Cui, Y.Q. Gu, and S. Achilefu, Folate-modified gold nanoclusters as near-infrared fluorescent probes for tumor imaging and therapy, *Nanoscale*, **4**(19), 6050-6064 (2012).
59. A. Retnakumari, S. Setua, D. Menon, P. Ravindran, H. Muhammed, T. Pradeep, S. Nair, and M. Koyakutty, Molecular-receptor-specific, non-toxic, near-infrared-emitting Au cluster-protein nanoconjugates for targeted cancer imaging, *Nanotechnology*, **21**(5), 055103 (2010).
60. W.J. Zhang, J. Ye, Y.Y. Zhang, Q.W. Li, X.W. Dong, H. Jiang, and X.M. Wang, One-step facile synthesis of fluorescent gold nanoclusters for rapid bio-imaging of cancer cells and small animals, *RSC Adv.*, **5**(78), 63821-63826 (2015).
61. Y. Pan, S. Neuss, A. Leifert, M. Fischler, F. Wen, U. Simon, G. Schmid, W. Brandau, and W. Jahnen-Dechent, Size-dependent cytotoxicity of gold nanoparticles, *Small*, **3**(11), 1941-1949 (2007).
62. J. Park, D.-H. Lim, H.-J. Lim, T. Kwon, J.-s. Choi, S. Jeong, I.-H. Choi, and J. Cheon, Size dependent macrophage responses and toxicological effects of Ag nanoparticles, *Chem. Commun.*, **47**(15), 4382-4384 (2011).
63. R. Coradeghini, S. Gioria, C.P. García, P. Nativo, F. Franchini, D. Gilliland, J. Ponti, and F. Rossi, Size-dependent toxicity and cell interaction mechanisms of gold nanoparticles on mouse fibroblasts, *Toxicol. Lett.*, **217**(3), 205-216 (2013).

64. B.S. Ramesh, E. Giorgakis, V. Lopez-Davila, A.K. Dashtarzheneha, and M. Loizidou, Detection of cell surface calreticulin as a potential cancer biomarker using near-infrared emitting gold nanoclusters, *Nanotechnology*, **27**(28), 285101 (2016).
65. A. Manke, L.Y. Wang, and Y. Rojanasakul, Mechanisms of nanoparticle-induced oxidative stress and toxicity, *Biomed. Res. Int.*, **20**, 942916 (2013).
66. P.P. Fu, Q.S. Xia, H.M. Hwang, P.C. Ray, and H.T. Yu, Mechanisms of nanotoxicity: Generation of reactive oxygen species, *J. Food Drug Anal.*, **22**(1), 64-75 (2014).
67. S. Steponkiene, D. Dapkute, U. Riekstina, and R. Rotomskis, Accumulation and distribution of non-targeted and anti-CD44-conjugated quantum dots in distinct phenotypes of breast cancer, *J. Nanomed. Nanotechnol.*, **6**(6), 1000341 (2015).
68. C.M. Fillmore and C. Kuperwasser, Human breast cancer cell lines contain stem-like cells that self-renew, give rise to phenotypically diverse progeny and survive chemotherapy, *Breast Cancer Res.*, **10**(2), R25 (2008).

Curriculum Vitae

Marija Matulionytė

Personal information

Date of birth: Oct 9, 1987
E-mail address: marija.matulionyte@gmail.com
Nationality: Lithuanian
Gender: Female

Education

2012 **Master of Science *Magna Cum Laude*** diploma in **Biophysics**, Vilnius University, Lithuania.
2010 **Bachelor of Science** diploma in **Physics** (Applied Physics), Vilnius University, Lithuania.

Internships

2012 02 – 2012 06 **Student Research Internship** at Vilnius University, Faculty of Physics (Vilnius, Lithuania).
Project „Investigation of spatial characteristics of gold nanoparticles using transmission electron microscopy“, supervisor Prof. dr. habil. R. Rotomskis.

2011 09 – 2011 12 **Student Research Internship** at Vilnius University, Faculty of Physics (Vilnius, Lithuania).
Project „Investigation of spatial properties of gold-protein nanoparticles using quasi-elastic scattering method“, supervisor Prof. dr. habil. R. Rotomskis.

2011 06 – 2011 09 **Pre-phD internship** at Linköping University (Linköping, Sweden).
Project “Interaction of insulin with quantum dots”, supervisor doc. dr. Niclas Solin.

2011 02 – 2011 06 **Research Internship** in Biomolecular and Organic Electronics group at Linköping University (Linköping, Sweden).
Project “Investigation on the preparation of functionalized bio-molecular materials”, supervisor Prof. dr. Olle Inganäs.

2010 10 – 2011 03 **Student research internship** organized by the Research Council of Lithuania under the project “Promotion of Students’s Scientific Activities”
Project „Investigation of spatial properties of superparamagnetic nanoparticles using atomic force microscopy“, supervisor Prof. dr. habil. R. Rotomskis.

Academic positions held & participation in projects

- 2014 01–present **Junior Research Associate** at the Laboratory of Biomedical Physics, National Cancer Institute, Lithuania.
- 2014 04–2015 05 **Junior Research Associate** at National Cancer Institute, Lithuania.
Scientific Research Project supported by the Republic of Lithuania
“Programming cells and management of tumor microenvironment for personal therapy in oncology–LASTER”.
- 2012 10 –2014 01 **Biophysicist** at the Laboratory of Biomedical Physics, Institute of Oncology, Vilnius University.
- 2009 10 –2010 06 **Junior Research Associate** at Institute of Oncology, Vilnius University.
Scientific Research Project supported by Norway grants and the Republic of Lithuania “Multifunctional nanoparticles for specific non-invasive early diagnostics and treatment of cancer”.

Languages

Lithuanian (*mother tongue*), English (*v. good*), Russian (*good*), French (*elementary*).

Computer skills

Microsoft Office, Corel, Origin, ImageJ, EZ-C1, EZ-C1 Free viewer.